NASA/TM-2012-217563
NESC-RP-09-00597

Assessment of Microphone Phased Array for Measuring Launch Vehicle Lift-off Acoustics

Roberto Garcia/NESC
Langley Research Center, Hampton, Virginia

April 2012

NASA STI Program . . . in Profile

Since its founding, NASA has been dedicated to the advancement of aeronautics and space science. The NASA scientific and technical information (STI) program plays a key part in helping NASA maintain this important role.

The NASA STI program operates under the auspices of the Agency Chief Information Officer. It collects, organizes, provides for archiving, and disseminates NASA's STI. The NASA STI program provides access to the NASA Aeronautics and Space Database and its public interface, the NASA Technical Report Server, thus providing one of the largest collections of aeronautical and space science STI in the world. Results are published in both non-NASA channels and by NASA in the NASA STI Report Series, which includes the following report types:

- TECHNICAL PUBLICATION. Reports of completed research or a major significant phase of research that present the results of NASA programs and include extensive data or theoretical analysis. Includes compilations of significant scientific and technical data and information deemed to be of continuing reference value. NASA counterpart of peer-reviewed formal professional papers, but having less stringent limitations on manuscript length and extent of graphic presentations.

- TECHNICAL MEMORANDUM. Scientific and technical findings that are preliminary or of specialized interest, e.g., quick release reports, working papers, and bibliographies that contain minimal annotation. Does not contain extensive analysis.

- CONTRACTOR REPORT. Scientific and technical findings by NASA-sponsored contractors and grantees.

- CONFERENCE PUBLICATION. Collected papers from scientific and technical conferences, symposia, seminars, or other meetings sponsored or co-sponsored by NASA.

- SPECIAL PUBLICATION. Scientific, technical, or historical information from NASA programs, projects, and missions, often concerned with subjects having substantial public interest.

- TECHNICAL TRANSLATION. English-language translations of foreign scientific and technical material pertinent to NASA's mission.

Specialized services also include creating custom thesauri, building customized databases, and organizing and publishing research results.

For more information about the NASA STI program, see the following:

- Access the NASA STI program home page at *http://www.sti.nasa.gov*

- E-mail your question via the Internet to help@sti.nasa.gov

- Fax your question to the NASA STI Help Desk at 443-757-5803

- Phone the NASA STI Help Desk at 443-757-5802

- Write to:
  NASA STI Help Desk
  NASA Center for AeroSpace Information
  7115 Standard Drive
  Hanover, MD 21076-1320

NASA/TM-2012-217563
NESC-RP-09-00597

Assessment of Microphone Phased Array for Measuring Launch Vehicle Lift-off Acoustics

Roberto Garcia/NESC
Langley Research Center, Hampton, Virginia

April 2012

Assessment of Microphone Phased Array for Measuring Launch Vehicle Lift-off Acoustics

March 22, 2012

NESC Request No.: 09-00597

Report Approval and Revision History

NOTE: This document was approved at the March 22, 2012, NRB. This document was submitted to the NESC Director on April 4, 2012, for configuration control.

Approved:	*Original Signature on File*	4/10/12
	NESC Director	Date

Version	Description of Revision	Office of Primary Responsibility	Effective Date
1.0	Initial Release	Mr. Roberto Garcia, NASA Technical Fellow for Propulsion, MSFC	3/22/12

Table of Contents

Technical Assessment Report

List of Figures

	Document #:	Version:
NASA Engineering and Safety Center **Technical Assessment Report**	**NESC-RP-09-00597**	**1.0**

Title:	Page #:
Assessment of Microphone Phased Array for Measuring Launch Vehicle Lift-off Acoustics	4 of 47

List of Tables

Technical Assessment Report

1.0   Notification and Authorization

A NASA Engineering and Safety Center (NESC) assessment was approved as an out-of-board activity on November 4, 2009. The assessment plan was approved by the NESC Review Board (NRB) on December 10, 2009. The final report was presented for approval on March 22, 2012.

The key stakeholders for this assessment are the lift-off acoustic community at Marshall Space Flight Center (MSFC), the mobile launch platform (MLP) acoustics engineering community at the Kennedy Space Center (KSC), the NASA Aerosciences Technical Discipline Team (TDT), and industry launch vehicle analysts interested in the development of this technique and application for lift-off environment. Additional stakeholders are the Multi-Purpose Crew Vehicle (MPCV) and Space Launch System (SLS) Programs.

2.0   Signature Page

Submitted by:

Team Signature Page on File – 4/16/12

_____

Mr. Roberto Garcia   Date

Significant Contributors:

_____

Mr. Jayanta Panda   Date

Signatories declare the findings, observations, and NESC recommendations compiled in the report are factually based from data extracted from program/project documents, contractor reports, and open literature, and/or generated from independently conducted tests, analysis, and inspections.

3.0   Team List

Name	Discipline	Organization
Core Team		
Roberto Garcia	NASA Technical Fellow for Propulsion	MSFC
Jayanta Panda	Primary Acoustician, NESC AeroSciences and Propulsion TDTs	ARC
Robert Mosher	Software & Test Support	Aerospace Computing, Inc.
Janice Houston	MSFC Engineering support	Jacobs Engineering
Dennis Strickland	MSFC Technical support	MSFC
Loutricia Johnson	MTSO Program Analyst	LaRC
Administrative Support		
Tina Dunn-Pittman	Project Coordinator	LaRC/ATK
Erin Moran	Technical Writer	LaRC/ATK

3.1   Acknowledgements

The assessment team greatly acknowledges the constant help from a large number of engineers and technicians led by Mr. Dennis Strickland (MSFC) in setting up the array, Ms. Allison Lee (MSFC) for help with the logistics of the operation, and Ms. Janice Houston of Jacobs Engineering for coordinating the test operations. The team would like to thank the MSFC team for the photographs used in Figures 7.2-2, 7.2-3, 7.3-1, 7.4-9, and 7.4-11.

4.0 Executive Summary

Usefulness of a microphone phased array to identify noise sources in applications involving rocket motors was verified using a 70-element, 0.25-inch-diameter sensor array in seven different tests of the Ares I Scale Model Acoustics Test (ASMAT). Many precautions were taken to protect the sensitive condenser microphones and camera equipment from the environmental elements during prolonged outdoor stay, exposure to the intense vibro-acoustics environment, debris, and water-spray during a motor horizontal hotfire test. In the first phase of the study, the array was placed in an anechoic chamber for calibration and validation of the indigenous Matlab®-based beamform software. In the next phase, the equipment was shipped to the Marshall Space Flight Center (MSFC), where the array hardware was rebuilt to safeguard electronic components. The first test involved a motor-only burn. The beamformed noise-source map was superimposed on an image of the rocket plume to readily identify the source distribution. It was found that the horizontally-fired motor plume made an exceptionally long, greater than 30-nozzle-diameter, noise source over a large frequency range. The array was found to be most effective in the frequency range of 2- to 10-kHz. For the next six tests, the array was set up in the vicinity of a 5-percent-scale model of the Ares I vehicle in a launch or vertical configuration. The tests involved static-firing at different model configurations representing various stages of lift-off, such as: (a) model at hold-down position; (b) model at different elevations with the accompanying lateral drift; (c) absence or presence of various water injection systems; and (d) absence or presence of a launch mount (LM). The beamformed plots show that, in almost all cases, impingement by the plume on various regions of the pad constitutes the primary noise sources. The scenario is different from the current models and expectations based on NASA SP-8072 [ref. 5] and its variations, which assumes the plume as the noise source and does not take into account the importance of impingement. It was found that another parameter, the sidewise drift of the vehicle with elevation, influenced the strength of the impingement noise sources, yet was not considered in the prediction methods. It was observed that the addition of water in the trench and in the hole of the mobile launch platform (MLP) attenuated noise sources radiating from these places. Water injection on the top of the MLP, "rainbird" system, produced some relief, but the impingement source remained active. The noise source maps suggest that the minimization of plume impingement by limiting the vehicle drift in the early part of lift-off, covering-up the trench as much as possible, and by removing extraneous components, such as the LM will lead to a reduction of the lift-off acoustics level.

5.0 Assessment Plan

The scope of this work was divided into two efforts. The first effort was the application of the phased array in a horizontal solid rocket firing to verify sensor survivability, to improve familiarity operations in the MSFC test area, and to verify the analysis software. The second effort was the application of the microphone phased array during six ASMAT firings.

The first effort was scheduled to be completed in fiscal year (FY) 2010, Year 1, while the second effort was for the FY2011, Year 2. In Year 1, the existing array was augmented, calibrated, tested, and verified at the Ames Research Center (ARC) acoustics facility. The data processing software was upgraded to a version that used deconvolution of the point-spread function (psf) to improve the imaging resolution. After completion of these tasks, the array was shipped to MSFC for participation in the horizontal motor firing test and the ASMAT firings.

6.0 Background

Significant advancements in sensor, data acquisition, and computing technologies, and recent progress in sharpening the noise source distribution via advanced processing techniques, have widened the usage of microphone phased array in recent years. The aircraft industry uses phased array for the identification of noise sources on airframes, engines, landing gear, and other aircraft parts [refs. 7, 8, 15]. Arrays are used to detect noise sources in automotive and manufacturing industries. The goal of the work was to extend the usage of this technology to spacecraft applications.

Perhaps the most obvious application is in launch acoustics where every part of a launch vehicle, launch pad, and a large number of components used for the ground operations are subjected to the high acoustics loads generated during lift-off. Even a couple of decibel (dB) reductions of the acoustic level translate into a sizable reduction of cost, weight, and risk of failure during qualification testing of a large number of components. The first step towards that end is the identification of the noise sources. The existing knowledge-base, available flight data, and the model-scale tests almost exclusively rely on single microphones that are unable to detect noise sources. Single microphones measure the local sound pressure; they are incapable of identifying the distant locations where the sound waves have originated. Alternatively, a phased array of a microphone is a "tuned listener" that can directly identify the locations of the noise sources.

The specific purpose of the present work was to demonstrate the suitability of a microphone phased array for launch acoustics applications via participation in selected firings of ASMAT. ASMAT is a part of the discontinued Constellation Program Ares I Project, but the basic understanding gained from this test is expected to help development of the SLS vehicles. Correct identification of sources not only improves the predictive ability, but provides guidance for a quieter design of the launch pad and optimization of the water suppression system.

	Document #:	Version:
NASA Engineering and Safety Center **Technical Assessment Report**	**NESC-RP-09-00597**	**1.0**

Title:	Page #:
Assessment of Microphone Phased Array for Measuring Launch Vehicle Lift-off Acoustics	10 of 47

The phased array operations need to be accomplished on a "least interference" basis relative to the baseline ASMAT activities. It was planned to mount the array on a removable stand that can be mounted close to the test stand and locked into its designated place prior to a test firing. Typically, the array needs to be placed in close vicinity to the subject affected by the noise. For the lift-off test, the critical component is the Orion crew module, which lies at the top-most part of the model. Therefore, it was desirable to identify sources radiating noise/ignition over-pressure (IOP) waves towards the top part. This assessment included support from MSFC personnel to help with various pre- and post-test setting up work.

The baseline plan for ASMAT was about 17 firings over the duration of 7 months. The team suggested acquiring phased array data in six of these firings to include the dry (i.e., no water) firing, several of the water injection optimization tests, a test with the scale vehicle at some elevation above the pad, and the worst ground acoustics environment case. Problems encountered with either data analysis software, instrumentation survivability, or the test-to-test instrument accuracy were documented and improvements demonstrated as much as possible during the test campaign. Verified data from each of these tests was analyzed and provided to the ASMAT team.

The launch acoustics part of the Ares I Project started with at least two different predictions of the environment. An examination of the prediction methodologies exposes the debates and doubts that arise from a poor understanding of the noise sources. Haynes & Kenny (2009) [ref. 2] used the procedure described by Eldred & Jones (1971) [ref. 5] with a small modification of the length of the plume-potential-core suggested by Varnier (2001) [ref. 4] for horizontal firing and a significant modification of a truncated plume length in the case of a deflected exhaust. Plotkin et al. (2009) [ref. 3] used a computer code that seems to carry most of the elements of the Eldred method (with additional features of scattering by the launch tower, and a different empiricism for the total noise [ref. 11]. The engineering methodologies were fundamentally pinned to an older model of noise-source distribution along a free plume. The presence of the elaborate launch pad was to make the plume bend at the location of the flame deflector (Figure 6.0-1).

		Document #:	Version:
NASA Engineering and Safety Center **Technical Assessment Report**		**NESC-RP-** **09-00597**	**1.0**

Title:	Page #:
Assessment of Microphone Phased Array for Measuring Launch **Vehicle Lift-off Acoustics**	11 of 47
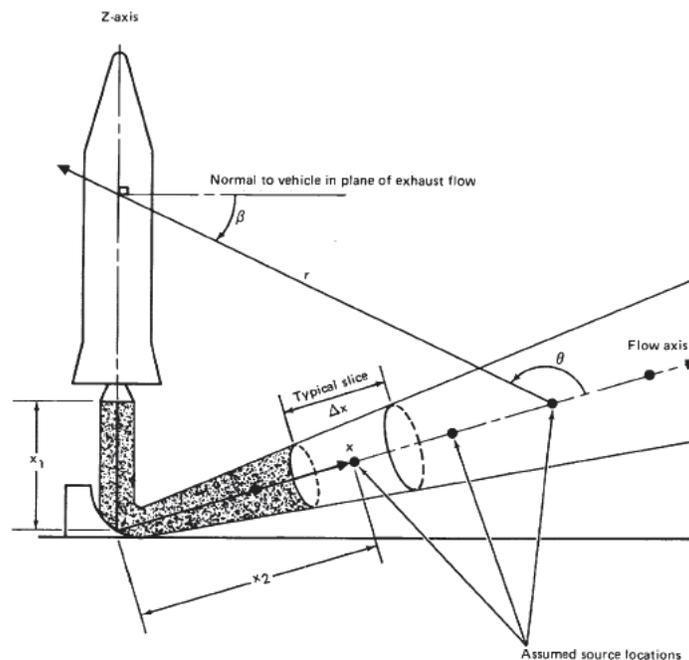
Figure 6.0-1. Model of Noise Source Distribution during Lift-off [ref. 5]

The shortfall of this model was that it overlooked the significant impingement zone on the flame deflector where, in almost all situations, impingement is known to cause much louder noise sources. Computational fluid dynamics analysis supported this deficiency [ref. 6]. Past efforts to compare the predicted spectra to those measured in flight indicated the true noise sources lay closer to the nozzle exit plane [ref. 12]. To overcome this shortcoming, empirical efforts have looked for an equivalent single point: the end of the supersonic core. Varnier (2001) [ref. 4] states, *"... the sound power peak location is related to the supersonic length of the flow, which appears to be the adequate reference length for a future jet noise model."* Sutherland (1993) writes *"The model applies the widely accepted concept that the dominant sound source for supersonic jet flow is close to, and downstream of, the supersonic tip."* The statement may have merit for a free-flowing plume, but is highly doubtful in a launch pad configuration where the plume is forced through a set of MLP holes, a deflector, and the trench. Nonetheless, the empirical effort to improve matching with the flight data led to the model of Haynes & Kenny (2009) [ref. 2], where the plume just after deflection was assumed to be the peak noise source (Figure 6.0-2).

Figure 6.0-2. Modifications for Predicting Ares I Lift-off Level [ref. 2]

Typically, the level of confidence on these predictions was not very high. Therefore, the ASMAT series using a 5 percent scaled model of the launch configuration was deemed necessary to improve the confidence in the predictions. During the test campaign, 18 static firings (including one motor-only burn) were conducted. However, the model positions were varied to represent vehicle locations at different time instances of lift-off. The original goal of ASMAT was to measure the acoustic and IOP levels on the vehicle, process-tower, and launch pad via individual microphone sensors. This report does not show data from these sensors. Instead, attention is confined to the results obtained from the deployment of the phased array instrumentation.

The first use of a microphone phased array to launch acoustics was by Gély et al. (2000) [ref. 9]. They used a 24-microphone, ring-array in a small-scale test of the Ariane 5 launch pad to identify sources responsible for the excessive low frequency noise in the payload fairing. No rocket motors were used for this test; instead, heated compressed air was used to simulate the rocket plumes. The beamformed maps correctly identified the sources, which led to various modifications, such as extending flue trenches and optimization of the water injection. The present application extends the array use from scaled simulations using heated air-to-direct measurement of solid-rocket plumes in launch pad configurations.

7.0 Data Analysis

7.1 Fundamentals of Beamforming using a Microphone Phased Aarray

A phased array images the sound sources by analyzing the wave phase front sensed by a large number of microphones. The individual microphone signals are delayed in time (or equivalently, in phase) and then added together. The first step in the imaging process is to divide the spatial zone (where the sound sources lie) into a large number of grid points, which are called the interrogation points (Figure 7.1-1). If there lies a noise source at one of the grid points, then the

estimated time delays (phase differences) for sound waves to reach the microphones are correct, and the summing process gives a large output. Alternatively, if the interrogation point is not a noise source, then the final sum is much lower. This principle makes what is known as the conventional beamforming, whereby a beamformed map is created over the interrogation region.
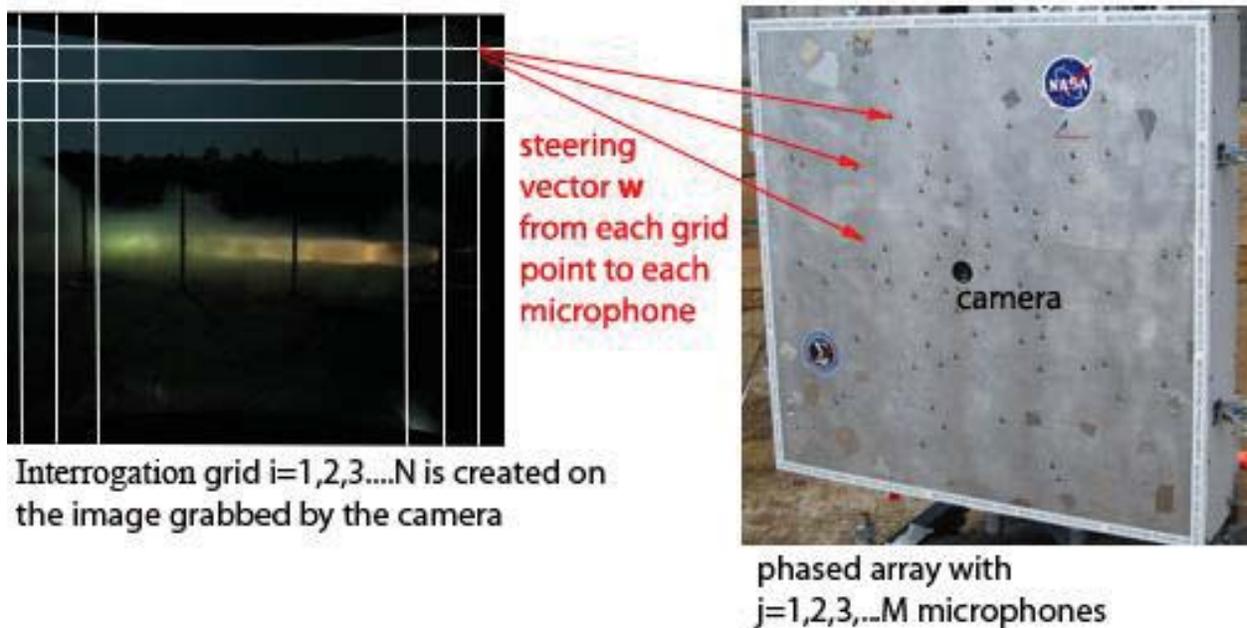
Figure 7.1-1. Schematic of the Steering Vectors for Beamforming

7.1.1 Conventional Beamforming

As shown in Figure 7.1-1, let j =1,2,3....N be the interrogation points in the region containing the noise source(s), and a phased array that contains $\ell = 1,2,3, \ldots$M number of microphones is used for the test. The radial distance from an interrogation point to an individual microphone $r_{j\ell}$ determines the phase shift and the relative amplitude measured by the microphone. The steering vector is a [Mx1] column matrix defined to incorporate these properties. It is given by the expression:

$$\boldsymbol{w_j} = \frac{\chi}{r_{j\ell}}\, e^{-\beta\, r_{j\ell}} \qquad (1)$$

where χ is a constant to normalize the steering vectors $\boldsymbol{w_j^\dagger}\boldsymbol{w_j} = 1$, β is the acoustic wavenumber $= \frac{2\pi f}{c}$, f is the frequency, and c is the speed of sound. The † symbol represents a complex-conjugate and transpose operation. The time traces of pressure fluctuations from individual microphones are Fourier transformed to obtain individual spectra $P_\ell(f)$. The cross-spectra between every pair of microphones are calculated and stored in a cross-spectral matrix (CSM) G.

Every element of the CSM is calculated as:

$$G_{\ell\ell\prime} = \langle P_{\ell}^* \, P_{\ell\prime} \rangle \qquad (2)$$

The * represents a complex conjugate and the $\langle \; \rangle$ represents an expected value (i.e., a time average over several seconds). Typically, the Fourier transform is performed over multiple overlapping blocks of data, which are then multiplied using equation 2 and finally averaged to obtain individual elements of the CSM. The diagonal elements of the CSM G_{11}, G_{22}, G_{33}, etc., contain the auto-spectra, which are contaminated by various spurious noise sources, such as that from the electronic. Setting the diagonal elements to zero improves the beamformed map.

The summing of the microphone signals (i.e., the elements of CSM) need to be preceded by a phase adjustment. These two steps are combined in a matrix manipulation, which leads to the beamform map, expressed by:

$$b_j(f) = \, w_j^{\dagger} G \, w_j \qquad (3)$$

The microphone weighting procedure was found to be useful in improving spatial resolution [ref. 8]. A linearly increasing weight W_{ℓ} based on the radial location R_{ℓ} of the microphone was used:

$$W_{\ell} = W_1 + (1 - W_1)R_{\ell}/R_0 \quad (4)$$

The constant W_1 was 0.1; R_0 represented radius of the outermost microphone. The final beamform equation utilizing the weight function is the following:

$$b_j(f) = \frac{w_j^{\dagger} W G_{diag=0} \, W^{\dagger} w_j}{(\sum W_m)^2 - (\sum W_m)} \qquad (5)$$

where W is a row matrix containing the terms W_{ℓ}. It is noted that equation 1 for the steering vector assumes that the noise sources radiate as monopoles. This basic assumption of the beamforming process has been under scrutiny for the history of the phased array technology. The justification for the assumption has been that little change in the beamformed map is obtained by assuming other types of sources. Moreover, in a lift-off environment there exist a variety of distributed noise sources and reflective surfaces, each with different directivity patterns. The possibility of making an error is minimized by assuming that the noise sources consist of a large number of monopoles. Therefore, the noise source results presented in this report are subjected to the inherent assumptions of the conventional beamforming process, namely the complex noise sources can be modeled as the sum of many monopoles, and sound propagation is strictly linear.

Interpretation of the noise-source maps obtained from a phased array requires familiarization with the fundamental property of the array response, described by its psf (Figure 7.1-2b). As the name implies, a psf describes how a point source becomes spread out in the beamform map. The spreading or smearing is dependent on the frequency of interest, the solid angle subtended by the

array, and the design of the microphone pattern. The psf at any point k in the beamformed region is calculated as:

$$psf_k(f) \; = \; \left| w_j^\dagger \, w_k \right|^2 \quad \textbf{(6)}$$

An examination of Figure 7.1-2(b) shows that at the low frequency end, the summed-up array output decreases slowly from the locations of the actual source to the neighboring regions. The extent of smearing is inversely proportional to the frequency of interest: worst for the lowest frequency. However, the strength and number of side lobes (that falsely makes the appearance of adjacent sources) is directly proportional to the frequency. More discussion on the measurement uncertainty is presented later in the report.
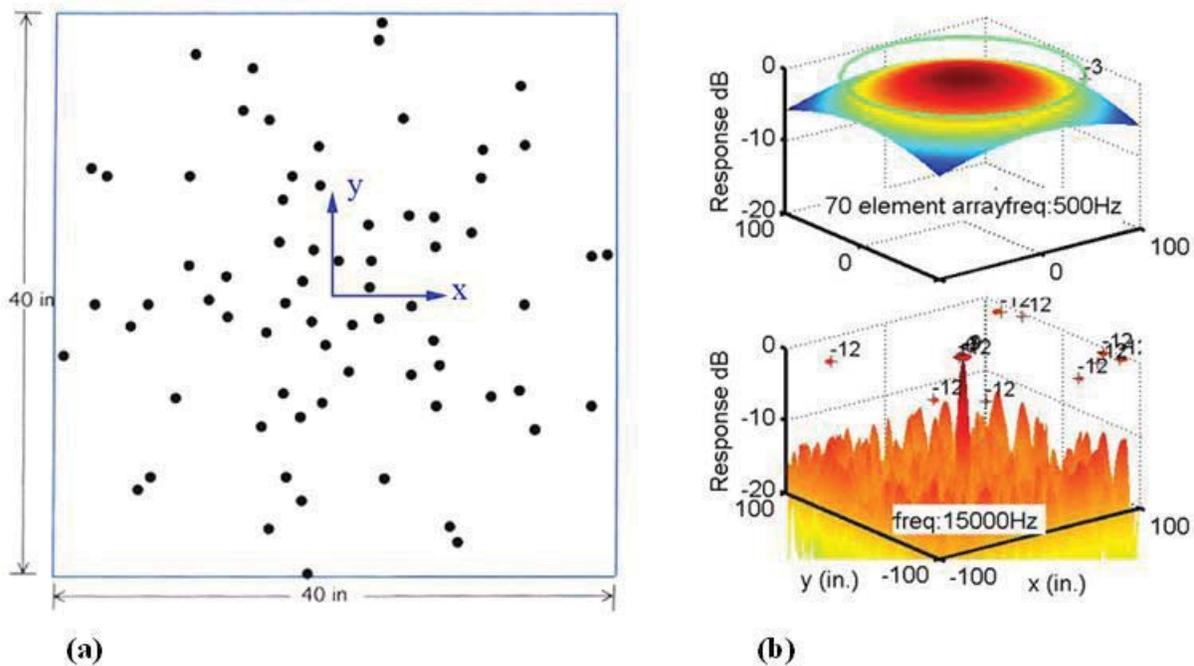
Figure 7.1-2. (a) Microphone Pattern on the Array Plate; (b) psf for the Two Indicated Frequencies for a Point Source Located at the Origin and z = 240 inches from the Plate

Recently, there have been multiple efforts to improve the array resolution by deconvolving the psf from the beamformed output. A summary of these methods applied for the present application and sample results are discussed in Appendix A.

7.1.2   Matlab® Implementation

The beamforming schemes were implemented in the commercially-available Matlab® platform. A quad-core personal computer (PC) and the Matlab® Distributed Computing Toolbox were used. Once the CSM was calculated, the rest of the beamforming operation was accomplished

quickly (a few seconds for each frequency bins). The CSM calculation took between 1 to 5 minutes, depending on the duration of the microphone data.

To facilitate direct identification of the noise sources, the interrogation grid for beamforming was created over an image of the region of interest. A camera was mounted at the center of the array and was used to capture video (at 7.5 frames per second) simultaneously over the duration of the microphone data recording. When the noise source is stationary, only one frame of the captured video was sufficient for further processing. The first step after selecting the frame was to perform a correction for barrel distortion due to the fish-eye lens used with the camera. The low focal length lens was useful to capture a large view angle. The expression used for making the correction was $s = r + ar^3$, where s is the true radius and r is the measured radius of each pixel from the center of the image. The correction factor 'a' was obtained by trial and error. In the next step, the images region was divided into a uniformly spaced grid. To select the number of grid points, the Rayleigh criterion was applied to the highest frequency of interest. According to this criterion, the minimum resolvable detail is due to the diffraction-limit of the array when the first diffraction minimum of the image of one source point coincides with the maximum of another. For a circular aperture of diameter d, the angular resolution in radians θ_R is directly related to the wavelength λ of interest.

$$sin\theta_R = 1.22\,\frac{\lambda}{d} \qquad (7)$$

For the present estimate, the maximum separation between any microphone pairs was assumed to be d. This equation shows that for a given array size, the angular resolution improves with frequency. Conversely, the highest frequency of interest dictates resolution of the interrogation grid. For the present application, a uniformly spaced grid of $1/10^{th}$ the array resolution at the highest frequency of interest was used. The conventional beamform calculations were applied on individual narrow bands of the CSM.

The beamform code was extended to create movies of the time-evolution of the noise sources. After ignition, the steady part of the motor burn lasted a couple of seconds. To capture the changes in source distribution over the entire burn, the time-series data from each microphone was pieced into 0.15-second segments, which corresponded to the camera frame rate of 7.5/second. The CSM was calculated on each segment followed by the conventional beamform calculations. The beamform map was plotted to the individual video frames and the created frames were animated to create a movie of the noise source evolution. Sample movies were presented at the NRB as supplementary information to this report.

7.2   Phased Array Hardware

The basic array plate containing the 70-element condenser 0.25-inch-diameter microphone array was designed for wind tunnel tests [ref. 15]. The present use in an outdoor rocket test facility required additional instrumentations and protection from exterior environmental conditions. The

array plate was modified to place a video camera at the center, with two dynamic pressure transducers (Kulite®) to measure impulse loading from the IOP pulse. The video camera at the center of the array, with a wide-angle 3.5-mm lens, was used to directly image the physical noise sources. The aperture of the video camera lens was remotely adjusted via a servo-controlled actuator; this allowed for adjustment for the variable day-light conditions and plume glare.

A weather-resistant case was built around the plate to protect the equipment from rain, snow, wind, and other elements. The case was made of three components: a cover plate for the front end, a back-chamber to protect the back side, and two junction boxes attached to the back-chamber to make a water-tight connection for the large number cables. The weather-resistant case, constructed of an aluminum frame, sheet metal, and polycarbonate boards, was sealed using weather strips and silicone sealants. The rear chamber held desiccants to maintain a dry environment. However, during a simulated rain test, it was found that the case was not completely water proof. This led to an addition of two more preventive measures. A plastic bag was placed over the weather-resistant case, and the rear chamber was continuously purged using dry missile grade air. All of these preventive measures were found to be effective through subsequent rain tests and ultimately during prolonged exposure at the test site when several rain, snow, and thunderstorms passed over the array hardware.

After the initial testing, calibration, and software validation at ARC (Figure 7.2-1), the entire phased array hardware was shipped to MSFC test stand TS116. There, the setup was rebuilt in two parts: the array box with all microphone and other sensors were mounted close to the model, and the electronic components (e.g., computer, data acquisition system, amplifiers, etc.) were placed indoors in an environmentally controlled room away from the test stand. There were 164-foot-long cables used to connect microphone preamplifiers to the amplifiers. At the array case, the cables were passed through rubber grommets at the junction-box to make water-tight connections. The long cable bundle was protected by split pipes.

The entire array setup was subjected to a non-interference criterion, where the operation of the phased array had to be completely independent and separate from the ASMAT primary test objectives. The non-interference condition prohibited locating the array closer to the model, which would have provided a straightforward means of comparing fluctuations measured on the model with that measured by the array. Nevertheless, the same sound sources identified by the array were expected to be radiating towards the vehicle model.

For the horizontal fire test, the array with the protection chamber was placed 15 feet away from the nozzle centerline (Figure 7.2-2). The primary reason for that location was to avoid interference with all other pole-mounted microphones and IOP sensors used in the test. The array bottom edge was elevated 2 feet above the ground surface, and the array was rotated about its y-axis by 30 degrees, so that the camera had a clear view of the entire plume. For all other ASMAT tests involving the model and the launch pad, the array chamber was mounted on a tower (Figure 7.2-3) about 15 feet away from the test stand and 16 feet above ground. The tower

was secured via outriggers bolted to the concrete floor. Additionally, tether cables were used to increase torsion rigidity of the assembly. The tower with the array chamber was erected typically on the morning of each test and taken down after the test. Before erecting the tower, the array protection chamber was opened and each microphone was inspected and calibrated.
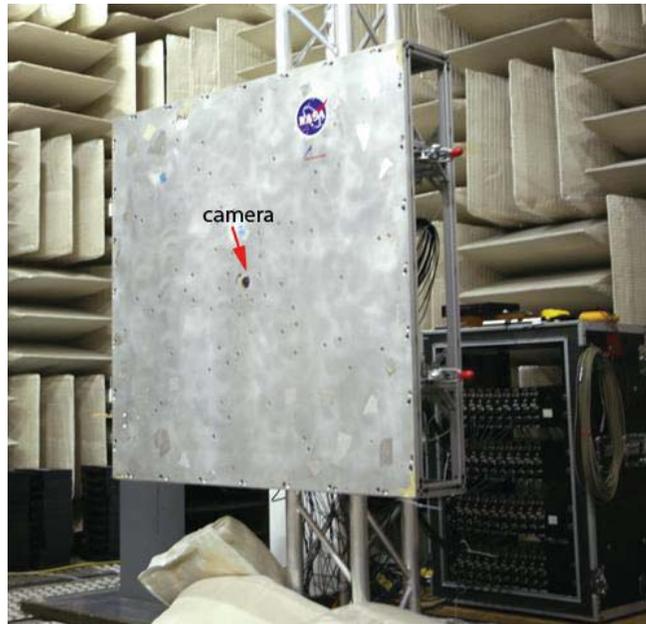
Figure 7.2-1. Phased-Array Inside an Anechoic Chamber

Figure 7.2-2. Phased-Array during a Solid Motor Firing in a Horizontal Test Stand
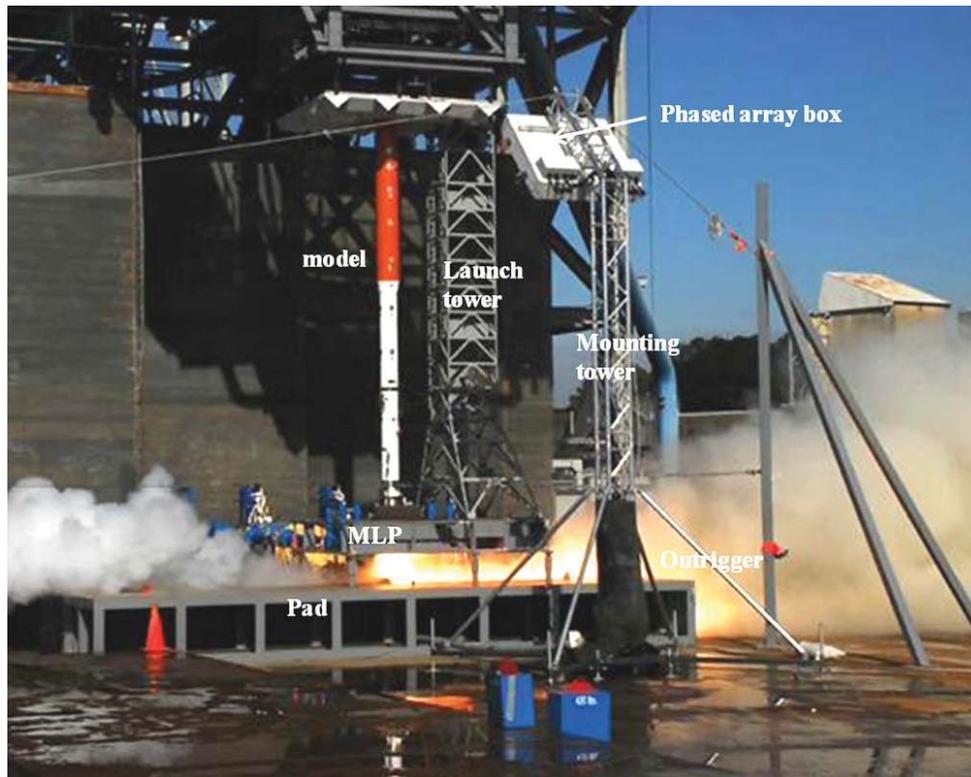
Figure 7.2-3. Setup of the Microphone Phased Array at the ASMAT Test Stand ASMAT3: Model at Hold-Down Position

A 72-channel, 16-bit VXI system was used for simultaneous acquisition of the microphone signals. The PC interfacing with the data acquisition system was accessed over a local network from the nearby control room. The same PC was used for capturing video signal from the array-camera, which was connected via a Fireware® extender. The data acquisition was started at t-10 second and lasted for 30 seconds. Each microphone channel was simultaneously sampled at 49152/second. The motor burn lasted for about 6 seconds, of which the first 2 seconds was full-power. Analysis of signals from the Kulite® transducers showed that the array plate was subjected to IOP wave with pressure rise of ~0.6 psi. The average acoustics level varied test-to-test in the range of 135 to 150 dB. The array plate experienced water-spray and debris impingement. However, the setup performed remarkably well over the year and a half of test duration; a total of about five sensors were lost. The most problematic part was that the VXI data acquisition system was found to be sensitive to temperature fluctuations requiring various components to be changed frequently. Problems due to vibration and variable light condition were fixed using better mounts and a camera aperture control system.

	Document #:	Version:
NASA Engineering and Safety Center Technical Assessment Report	**NESC-RP-09-00597**	**1.0**

Title:	Page #:
Assessment of Microphone Phased Array for Measuring Launch Vehicle Lift-off Acoustics	20 of 47

7.3   Test Facility

ASMAT was conducted at MSFC test stand TS116. It used a uniformly-scaled (5 percent) launch pad, MLP, launch tower, and a simplified model of the Ares I vehicle (Figure 7.3-1 and Figure 7.3-2). The launch pad was similar to that used for the Space Shuttle Program (SSP) with two trenches and a center flame deflector. The single plume of the Ares I solid rocket booster (SRB) impinged on one side (SRB-side) of the deflector. The MLP configuration was somewhat different from that of the SSP with one exhaust hole and the addition of a LM between the hole and the SRB nozzle exit. Among other purposes, the LM was expected to confine the plume within the exhaust hole. Part way through the test, it was concluded that the LM did not help the acoustic environment and reduced the effectiveness of the on-deck water injection system. This led to the LM removal.

Figure 7.3-1. Front View of the ASMAT Test Setup

Figure 7.3-2. Side View of the Test Setup

The launch tower stood between the Ares I vehicle and the exhaust plume flowing through the trench. The intention of this arrangement was to provide some blockage to the acoustic path. This perhaps germinated from the noise source map model in common use [ref. 5] (Figure 6.0-1). The in-line vehicle was modeled by a cylinder with a variable diameter corresponding to the different zones of the full-scale vehicle. A solid rocket motor with ~10,000 lbf thrust was used to model the first stage booster. At the hold-down condition, the plume from the booster flowed through the LM and MLP exhaust holes to one side of the flame deflector, and finally flowed out of the trench. Note that similar to the SSP launch pad, there is a gap between the bottom of MLP and the top of the trench. No part of the plume came out of the rectangular cutout in the metallic structure of the MLP as seen in the side view of Figure 7.3-2.

	NASA Engineering and Safety Center	Document #:	Version:
	Technical Assessment Report	NESC-RP-09-00597	1.0

Title:	Page #:
Assessment of Microphone Phased Array for Measuring Launch Vehicle Lift-off Acoustics	22 of 47

The effectiveness of a variety of different water suppression systems was evaluated during the ASMAT series. There were two sets of water systems: one specifically targeting the IOP that appeared as soon as the solid motor was ignited, and a second system to reduce the overall acoustic levels. The second system is relevant for the present purpose. Similar to the SSP launch pad (Figure 7.3-3), there were three parts to the acoustic suppression system: "hole water": water injection through the hole in the MLP; "trench water": water injection inside on the deflector and inside of the flame trench; and "rainbird": water injection on the top of the MLP.
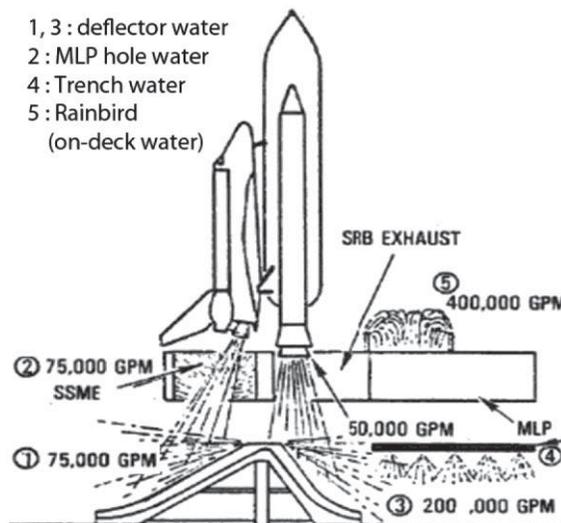
Figure 7.3-3. Sound Suppression System Employed for the SSP

The system used for the ASMAT test had similar subsystems. The primary differences were: only the SRB side of the deflector was used for passing the single plume of the Ares I booster; there was only one hole on the MLP; the rainbird system was relocated around the MLP hole; and the "trench water" was utilized.

Besides the horizontal firing, there were 17 vertical tests. The array was used in six vertical tests, plus the horizontal motor only test. The first vertical test, ASMAT 3 represented a hold-down condition when the vehicle was on the pad during the ignition of the first stage booster. For the rest of the ASMAT tests, the model was elevated to replicate different vertical positions of the vehicle. A critical element of the lift-off process is the sidewise drift that accompanies vehicle elevation. ASMAT replicated maximum expected drift of Ares I for most of the test conditions. In Table 7.3-1, the elevation and drift values are non-dimensionalized by the nozzle exit diameter D_{exit}. In ASMAT 17, a situation was tested where the vehicle elevation involved no drift, such that the plume mostly passed through the hole in the MLP deck. Additionally, all water injection systems were turned off. The hole and the trench water were turned on in ASMAT 11, and all three systems (hole, trench, and rainbird) were used in ASMAT 12. Note

that in ASMAT 11 and ASMAT 12, the model was moved sidewise (drifted). Therefore, a straightforward comparison with the ASMAT 17 was not possible. There were several cases tested to verify the effectiveness of the on-deck water injection, where the phased array could be used with ASMAT12.

Table 7.3-1. Part of the Test Matrix where Phased Array was Used

Test Name	Elevation H/D_{exit}	Drift Y/D_{exit}	Trench H_2O (gpm)	Hole H_2O (gpm)	On-deck H_2O (Ww/Wp)*	Comment
Horizontal	n/a	n/a	n/a	n/a	n/a	
ASMAT 3	0	0	0	0	0	With LM
ASMAT 4	3.9	0.61	873	291	0	With LM
ASMAT 7	7.9	0.9	873	291	0	With LM
ASMAT 11	8.6	0.9	873	291	0	No LM
ASMAT 12	8.6	0.9	873	291	4.5	No LM
ASMAT 17	8.6	0	0	0	0	No LM

*Ratio of mass fluxes: water flow to propellant flow

7.4   Results and Discussions

7.4.1   Validation of the Array Performance

The initial system check, calibration, and software validation were performed in the ARC acoustics laboratory. Additional in-situ validations were performed before every test at the ASMAT test stand. Sample results from these two sets of validations are discussed below.

For the initial system check the array was mounted inside an anechoic chamber (Figure 7.2-1). At first, the camera was calibrated to associate angular positions in x-z and y-z planes with the individual pixels. Knowledge of the perpendicular distance (z-distance) from the object plane to the phased array provided the x- and y- coordinates of every pixel in the image. The camera calibration was followed by an end-to-end calibration of individual microphones using a pistonphone. Finally, validation data were obtained by positioning a set of three speakers and driving them using separate broadband white noise generators. Each microphone channel was checked for phase anomaly. Figure 7.4-1 shows a sample result from a three-speaker setup where the speakers were equally spaced at 31-inches apart and at z = 176 inches from the array center. The beamform-map is superimposed on a video frame to help identify individual sources. The "drawn curtain" appearance of the image was due to the correction applied to remove barrel distortion. An examination of Figure 7.4-1 shows that, for the present arrangement, the conventional beamforming was unable to resolve individual speakers at the two lower frequencies, while they were identified at the two higher frequencies. At the highest, 15-kHz frequency side lobes appeared, which gave the appearance of pseudo-sources. It is

interesting to note that Rayleigh criterion of equation 7 places the minimum resolvable frequency at around 2.3 kHz for the speaker positions; the present array architecture and the beamforming software were found to provide a small improvement (i.e., 85 percent of Rayleigh resolution).
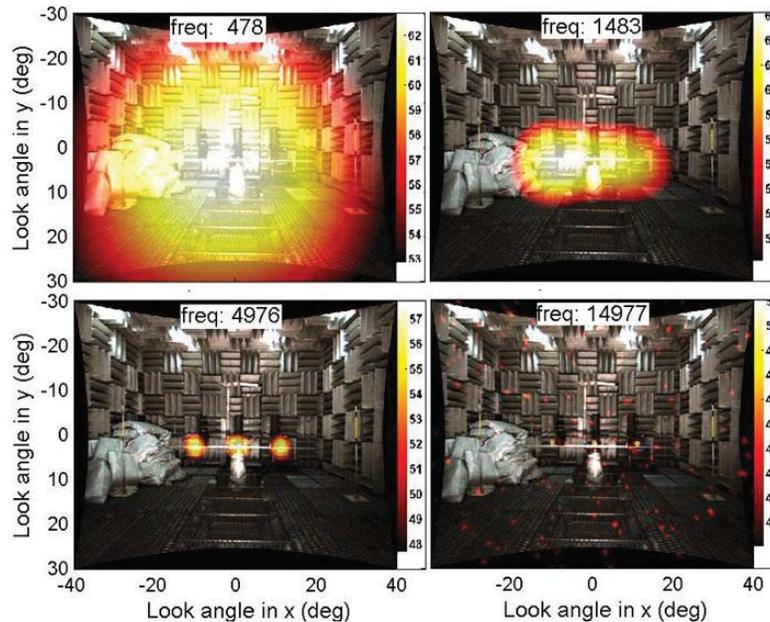
Figure 7.4-1. Beamformed Maps of Three-Speaker Sources in an Anechoic Chamber
The color scales represent source strength in a 96-Hz wide frequency band centered at the indicated frequencies.

Attempts were made to apply some of the advanced beamforming algorithms to improve the spot size at the low frequency and to reduce the side lobes at high frequencies (see Appendix A). Typically, such procedures were found to work well for compact noise sources. However, other difficulties arose for different algorithms when attempts were made to use with the rocket test data. The test stand created a reverberant environment and the noise sources were distributed; both of these seemed to create various problems in the attempt to deconvolve psf. Other investigations are in progress to achieve this goal. For this report, only conventional beamform data are presented.

Finally, there is a need to discuss uncertainties in the absolute magnitude of the noise sources. Note that the color scale next to each figure of the beamformed map shows the magnitude of the noise sources as measured at the array location. Typically, the color scale covers the peak 10-dB range of the sources. The uncertainties in these numbers arise due to three reasons: the inherent convolution of the true noise source with the array psf; the short duration of the motor burn; and a loss of coherence among microphone pairs. The first reason was discussed earlier. The steady part of the motor burn typically lasted for 2.2 seconds (Figure 7.4-2a), which was used for most of the beamformed results. The relatively short duration of the sample implied

fewer available cycles at the lower frequencies and increased side-lobes at the high frequencies. This is the second reason for uncertainties. The third reason is the inherent nature of the distributed noise sources. Data gathered from ASMAT tests showed a progressive loss in coherence for sensor pairs with longer separation distances. This loss was found to increase with frequency (Figure 7.4-2b). Therefore, the averaging process of the beamforming technique led to source strengths that were lower than the levels seen in the auto-spectra. No attempts were made to compensate for this loss. Nevertheless, the limitations are similar between two ASMAT configurations. Although there is a higher level of uncertainty in the absolute magnitudes of the noise sources, the relative differences between any two cases is believed to be reliable, and within a fraction of a dB. Therefore, the beamformed maps should be used for a comparative study among various ASMAT configurations.
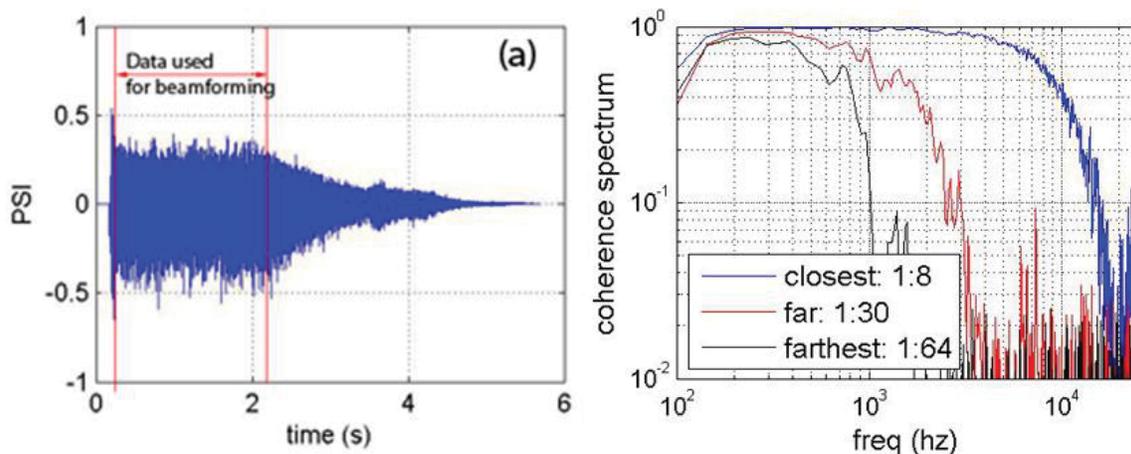
Figure 7.4-2. (a) Time Trace of Pressure Fluctuations from one of the Microphones in the Horizontal Motor Test; (b) Coherence Spectra Between indicated Pairs of Microphone

Figure 7.4-3 shows in-situ validation obtained from the ASMAT test stand where a single speaker was located at a corner of the launch pad. Recall that the array was about 16 feet above ground with a ~45-degree angle. The background image was captured by the video camera at the center of the array box. Similar to the prior figure, smearing of the source was progressively reduced with an increase of the beamform frequency while the number of the pseudo-sources increased with frequency. A large number of reflective surfaces were around the model. Besides the concrete floor and the metallic pad, there were steel blast curtains on the backside of the model.

	Document #:	Version:
NASA Engineering and Safety Center Technical Assessment Report	**NESC-RP-09-00597**	**1.0**

Title:	Page #:
Assessment of Microphone Phased Array for Measuring Launch Vehicle Lift-off Acoustics	26 of 47

Figure 7.4-3. Validation of the Phased Array Operation via Identification of a Single Speaker Source (at the bottom-left corner; the four plots are for the indicated four different frequencies)
The color scales show sound pressure levels over a 48-Hz wideband centered at the indicated frequencies.

The presence of these reflective surfaces created images of the noise source and increased the population of pseudo-sources (side-lobes). The "sweet range" was found to be between 2 and 6 kHz, where the array resolution was reasonably good and the pseudo sources were mostly lower than 10 dB. Most of the ASMAT test data presented in this report is in this frequency range. Using plume properties for Strouhal frequency calculations, 2.5 and 5 kHz correspond to $St = fD/U$ of 0.2 and 0.4, respectively. Strouhal numbers are used for the remainder of the figures in this report.

7.4.2 Horizontal Rocket Motor Only Test

The setup used in the horizontal test was discussed with Figure 7.2-2. Unlike the image in that figure, the camera at the center of the array plate captured a better image of the plume (Figure 7.4-4a). This frame, from the initiation of the burn, shows a clear periodic shock pattern present in the under-expanded plume. The glow in the plume was due to afterburning. The smoke was believed to be mostly made of aluminum oxide powder. The three vertical lines are the poles used for holding microphones for a separate suit of instrumentation.

Figure 7.4-2 shows a microphone time signal, and auto and cross-spectra collected from the horizontal test. Note that the spectra have double humps, separated by a dip, such features are indicative of interference from distinct sources. Conventional beamform results are shown in

Figure 7.4-4(b). The first observation is that there exist two distributed noise sources: one along the plume and the other is a reflection on the concrete test floor. The concrete pad acted as a mirror to the plume sources. It is obvious that any attempt to make free-field acoustic measurements in a horizontal rocket stand needed to pay attention to this reflection that nearly doubled the true amplitude.
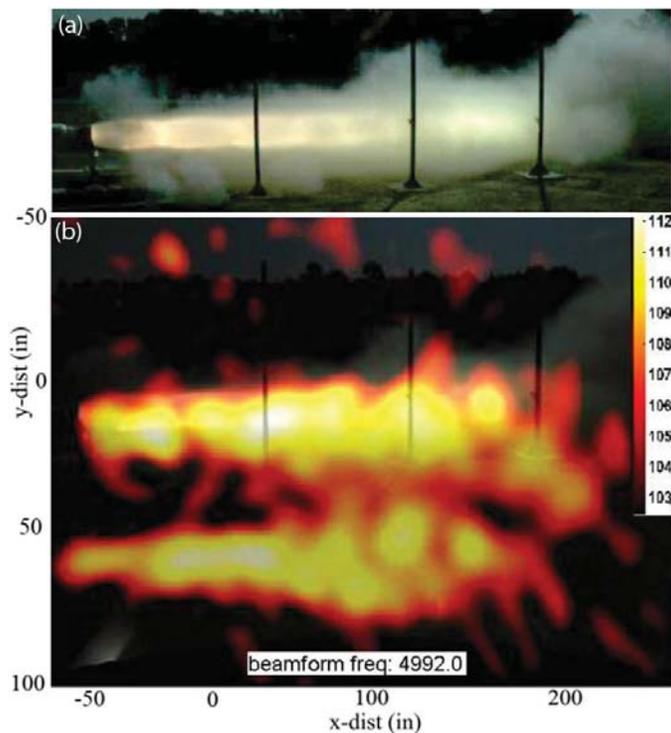
Figure 7.4-4. (a) The Plume of a Solid-Rocket Motor Fired Horizontally over a Concrete Pad; and (b) Noise Source Distribution at indicated Frequency as Measured by the Phased Array

Another interesting observation was the long spatial extent (greater than 30 diameters) of the noise sources that extended to the end of the visible afterburning core of the plume. The quasi-periodic shock pattern of the plume was found to create periodic modulation of the noise source. An examination of the source maps at other frequencies (not shown) showed the peak in the source distribution progressively moved closer to the nozzle exit with an increase in frequency. However, the downstream extent of the sources remained almost independent of frequency.

Supplementary material, video file "Horizontal.avi"

The time-lapsed video showed evolution of the noise sources from ignition to termination of the Rocket-Assisted Take Off (RATO) motor. It substantiated the effectiveness of the phased array in following the time varying noise source. At the end of the burn, as the plume became shorter, so did the distribution of noise sources. The reflected noise source followed suit.

7.4.3   Vertical Tests with Model of Ares I Vehicle

ASMAT 3

Figure 7.4-5 shows the distribution of the noise sources at four different frequencies for a hold-down condition (i.e., at zero elevation). No water was used for this test. An image of this test showing the locations of the hot plume and the position of the array is shown in Figure 7.2-3. The background image of Figure 7.4-5 was collected before the test by the camera at the center of the phased array. As expected, the source distribution at the lowest frequency, $St = 0.08$ (1 kHz), was excessively smeared due to the low resolution of the array. While at the highest frequency, $St = 0.8$ (10 kHz), the multitudes of side-lobes were artifacts of the beamforming process. The best balance between the two extremes, the "sweet-spot," are the maps at $St = 0.2$ (2.5 kHz) and 0.4 (5 kHz).
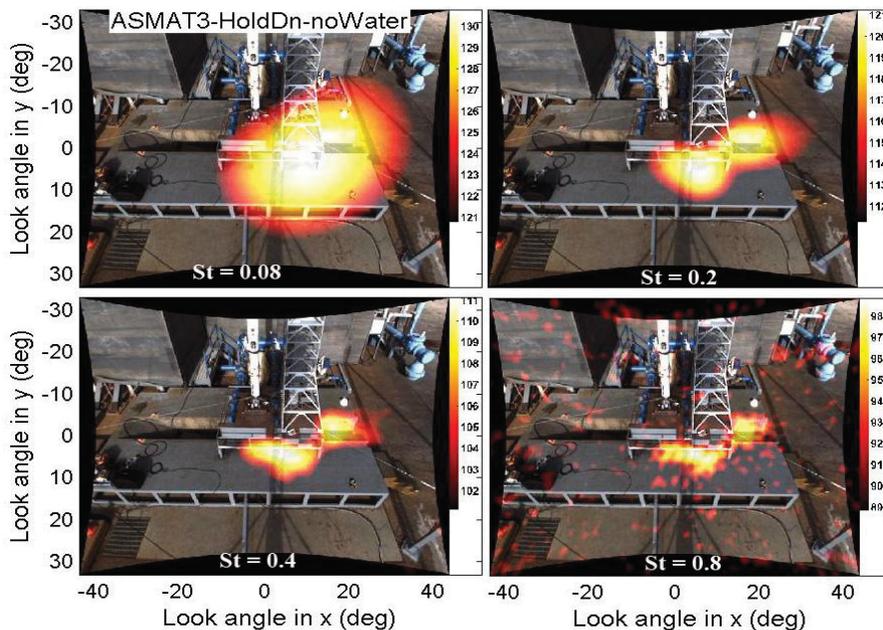
Figure 7.4-5. Beamformed Noise Sources at Four indicated Frequencies. ASMAT3: Model is at Hold-down Position, without Water Injection, and LM is in Place
The color scales show sound pressure levels over a 48-Hz wideband centered at the indicated frequencies.

Figure 7.4-5 identifies two strong sources: the gap between the MLP and the trench, and the open part of the flame trench on the right-side of the launch tower. An image of these two regions can be seen in the side view of Figure 7.4-6. Additional video footage taken during the test verified the flow of hot gas through the trench in absence of trench water. This hot plume and its impingement on the deflector are believed to be the origin of the two sources. There was no leakage of hot plume coming out of the gap between the MLP and the trench. Therefore, it is

believed that the first part of the identified sources originated inside the trench, and then spilled out through the gap between the MPL and the trench. Note that this gap existed on all four sides. Therefore, the vehicle model was expected to be exposed to sound radiation from all sides. A phased array detects only those sources radiating towards the array surface; that is why the beamformed plots of Figure 7.4-5 identifies only the front side of the MLP as the source. Closing the gap between the MLP and the trench should reduce the acoustic level experienced by the vehicle at the hold-down condition.

An important observation can be made by comparing the noise source model of Eldred-Jones (Figure 6.0-1) [ref. 5] and the measured source distribution of Figure 7.4-5. The rocket plume shot out of the right-hand-side trench exhaust. The Eldred-Jones model [ref. 5] assumes the entire plume length to be the noise source, while the beamformed map shows that the peak 10-dB range of the source are confined within the trench. The presence of the second source at the MLP pad gap could not be envisioned from the Eldred-Jones formulation [ref. 5]. The difference between the Eldred-Jones model [ref. 5] and the source distribution became more distinct in the subsequent tests.

Figure 7.4-6. Flow of Hot Gas through the Trench
(Image Fusion visualization, courtesy: Louise Walker, UARC and ARC)

Supplementary material, video file "ASMAT3.avi"

The video footage confirmed the description of the sources during the steady part of the burn. During the later part of the video, when the motor progressively tapered off, the noise sources weakened. First, the source at the open part of the trench disappeared, followed by the sources

around the MLP pad gap. At the end of the burn, the peak source moved to the nozzle exit, on the top of the LM, but the source strength was lowered by >30 dB.

ASMAT 4

An image of the ASMAT 4 test is shown in Figure 7.4-7(a). For this test, the model was lifted by $3.9D_{exit}$ above the LM, thereby exposing a part of the plume above the launch pad. More importantly, the model was drifted towards the launch tower by about $0.61D_{exit}$. This allowed part of the plume to spill out of the hole and impinge on the LM, MLP, and the base of the launch tower. The lift-off trajectory for the Ares I vehicle dictated this drift; the model-scale static test replicated this scenario. Figure 7.4-7(b) shows the off-center location of the nozzle exit with respect to the LM. The other significant part of the test configuration was the water injection. A large volume of water was injected inside the trench and the MLP hole, and on the top of the flame deflector via ducts built on the pad. The water flow was initiated before motor ignition and continued after the completion of the burn.

Figure 7.4-7(a). *Sparks Fly Off the Plume Impingement Point on LM and MLP in ASMAT4: Model Lifted by $3.9D_{exit}$ above the MLP*

Figure 7.4-7(b). *Closer View showing Drift to the Right of the LM/MLP Hole*

Figure 7.4-8 shows the noise source locations identified at three different frequencies. Unfortunately, the video obtained from the array-camera was underexposed. However, the outline of the trench and the MLP were visible. The bottom part of the model is visible as the white strip at the top center of each image; as marked, and the nozzle exit lies just below this

strip. An examination of the source maps shows that the primary noise source extended from one side of the LM to the base of the tower. This was the region where the plume from the rocket motor impinged on the pad. The beamformed source map shows that the impingement of the plume is responsible for most of the noise generation. Note that a large part of the plume passed through the trench. However, unlike ASMAT 3, water injection inside the MLP hole and the trench weakened the source so much that it was not visible in the top 10-dB range shown. Finally, the noise map has no resemblance to the Eldred-Jones model [ref. 5] of Figure 6.0-1, which missed the impingement zones as lift-off noise sources. The team believes that the Eldred-Jones model misses many other aspects of the noise path and source distribution. To improve comparison with flight and test data, the model makes an empirical assumption of reduction in noise generation efficiency of a deflected plume.
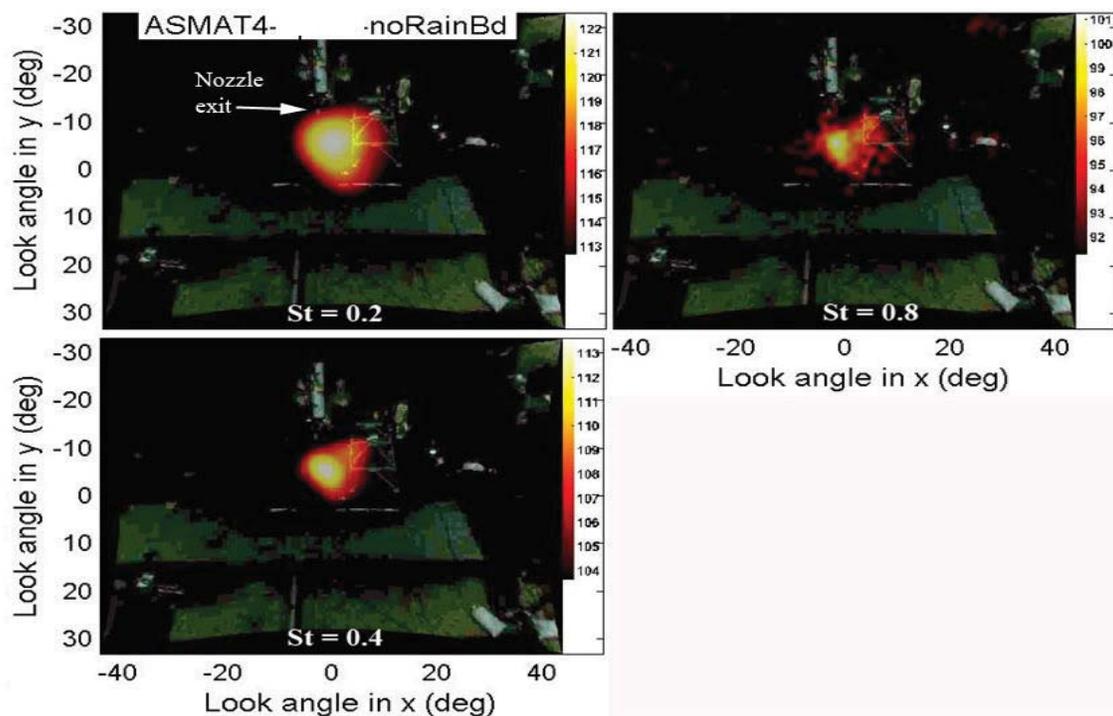
Figure 7.4-8. Beamformed Noise-Sources at the indicated Frequencies Measured in ASMAT 4

Supplementary material, video file "ASMAT4.avi"

The noise sources during the steady part of the burn are the same as previously described. As the plume weakened, so did the impingement source. At the very end of the burn, the source moved up and stayed around the nozzle exit.

ASMAT 17

In ASMAT 17, the sound suppression systems were turned off (completely dry), and the model was held at $8.6D_{exit}$ above the MLP platform. Additionally, there was no sidewise drift, so that the maximum possible part of the plume was passing through the MLP hole. Figure 7.4-9 is a frame from a video camera that captured a side view of the motor burn. This figure shows the bare part of the plume (seen through the support tower) above MLP, and the exhausting hot gases through the trench. The beamformed maps of Figure 7.4-10 show a U shape. A closer examination revealed that the noise sources were at three connected regions: like ASMAT 3, the gap between the MLP and the trench; like ASMAT 3, the open part of the flame trench on the right-side of the launch tower; and unlike ASMAT 3, the region around the MLP hole. The absence of hole and trench water brought the first two sources back to prominence. The third region was due to the plume impingement around the hole of the MLP deck. The hole was designed to be small to minimize IOP reflection. Despite no sidewise drift of the model, the edges of the plume impinged on the rim of the hole and created the loudest noise source. Note that the background image used to superimpose the beamformed map in Figure 7.4-10 was from a video taken before the motor ignition. Note the ladder, man-lift, amplifiers, etc., were removed before the test.

Figure 7.4-9. Side View of the Model and the Launch Pad in ASMAT 17
(no water, elevation =8.6 D_{exit}, drift = 0)
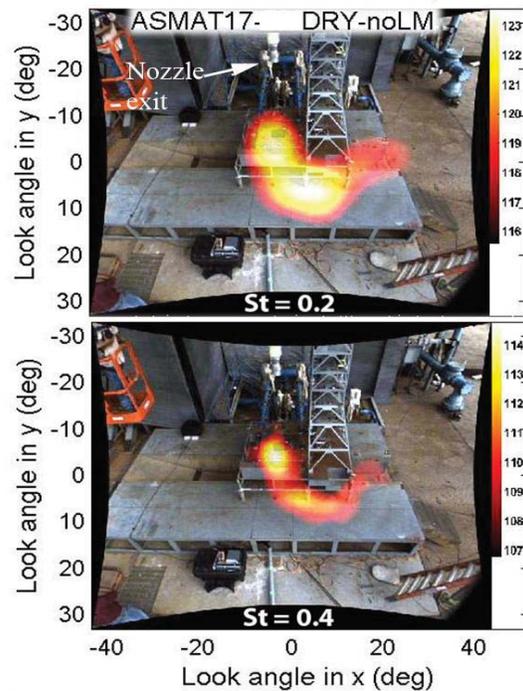
Figure 7.4-10. Beamformed Noise Sources from ASMAT 17 at indicated Two Frequencies

Supplementary material, video file "ASMAT17.avi"

This video provided the clearest indication that the plume was a weaker (at least by 10 dB) source than the rest described above. At the end of the burn, when all three of the identified sources disappear, the plume region increased in the source map. This showed that the prime part of the burn plume created noise sources that were below the 10-dB plot range.

ASMAT 11

The hole and the trench water system were turned on in ASMAT 11. The model was kept at the same elevation, but was drifted per trajectory information. Figure 7.4-11 is a front view of the test articles with the phased array setup in the foreground. The beamformed maps, shown in Figure 7.4-12, provide the clear indication of the effectiveness of the water system: the trench and the gap around the MLP are no longer in the source maps and the gap is no longer the primary issue. However, compared to ASMAT 17, a larger part of the plume impinged on the deck resulting in an increase of the peak source strength (see color bar). In other words, compared to ASMAT 17, the spatial extent of the sources is much smaller, yet the peak level is higher.

Figure 7.4-11. Photograph of ASMAT 11 (drift = 0.9D$_{exit}$, elevation = 8.6D$_{exit}$, hole and trench water)
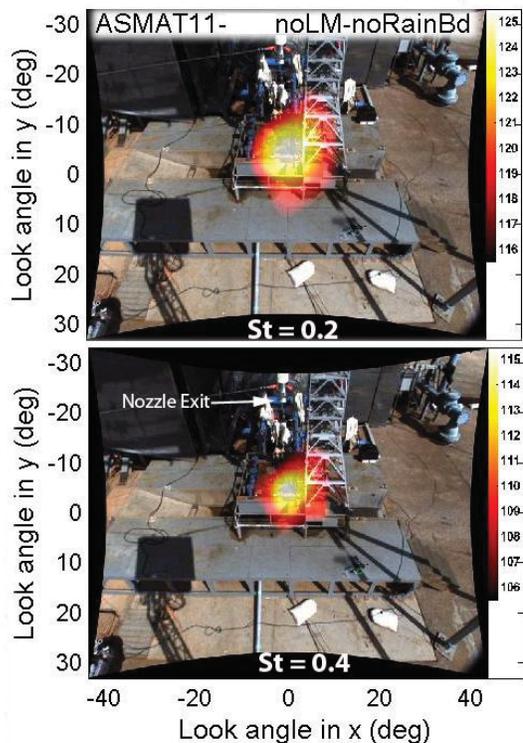
Figure 7.4-12. Beamformed Noise Source Maps at indicated Frequencies from ASMAT 11

Supplementary material, video file "ASMAT11.avi"

Similar observations, as described with the ASMAT17.avi file, can be made from this video.

ASMAT 12

All three parts (hole-water, trench-water, and rainbird) of the water suppression system were turned on in ASMAT 12. The vehicle elevation and drift were the same as in ASMAT 11. A large flow of water was used for this test. The mass flow of water was 4.5 times the propellant mass flux. Unlike a nominal lift-off situation, the rainbird system was turned on before the motor ignition. So, there was a pool of water accumulated on the top of the MLP when the motor was ignited. Figure 7.4-13 shows the plunging of the plume in this pool resulted in a large splash of water. A comparison of the microphone time traces between this and ASMAT 11 is shown in Figure 7.4-14 and shows observable attenuation of the acoustic level. The 0.02-second pressure traces (shown in Figure 7.4-14 (b) and (d)) show that the "N-waves" in the Mach wave radiation were particularly affected; the high positive peaks of the sound waves show good attenuation from the rainbird water. Figure 7.4-14(c) indicates a time-dependent attenuation. After ignition, when the plume plunged into the accumulated pool, there was a large attenuation. However, the levels increased significantly (after a fraction of a second) when the accumulated pool evaporated and the plume impinges on the MLP deck. In a nominal launch, the distance between the nozzle exit and the MLP deck would continuously increase and the time-dependent interaction between the plume and water deluge is likely to be different. The beamformed maps shown in Figure 7.4-15 identify compact noise sources around the impingement point. A benefit of the rainbird system is that it attenuates peripheral sources that may be caused by the deflected part of the plume re-impinging on the service tower. Nonetheless, the peak source strength in Figure 7.4-15 is only a couple of dB lower than that of no rainbird case (Figure 7.4-12).


Figure 7.4-13. Photograph from ASMAT 12: Rainbird (on-deck) Water Injection
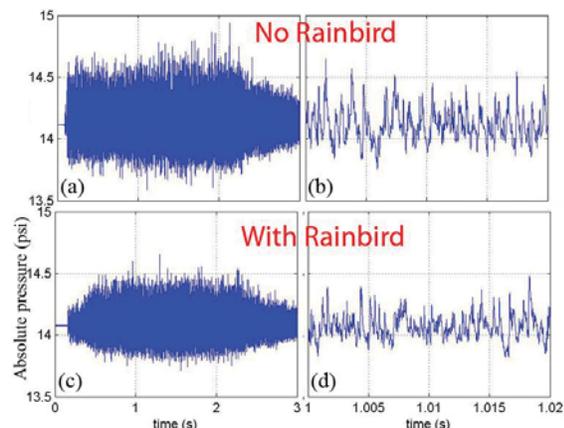
Figure 7.4-14. (a, b) Time Traces from an Absolute Transducer on the Array Plate, (c) ASMAT 11, (d) ASMAT 12

***Figure 7.4-15. Beamformed Noise Source Maps at the indicated Frequencies from ASMAT 12
(drift = 0.9D_exit, elevation = 8.6D_exit, hole, trench, and on-deck water)***

Supplementary material, video file "ASMAT12.avi"

Similar observations as described with ASMAT17.avi file can be made from this video. Discussions are centered on the location and strength of the noise sources as seen by the phased array. The acoustic levels are due to an integration of radiation from all such sources. A comparison of the acoustic spectra from the five ASMAT tests discussed is shown in Figure 7.4-16. Each spectrum in this figure is an average from all 70 microphones present in the array. It was difficult to make a direct comparison since more than one parameter was changed between most pairs. However, a comparison between the no-LM cases (i.e., ASMAT 17, ASMAT 12, and ASMAT 11) showed that the water suppression system produced attenuation in almost all frequency ranges. Compared to ASMAT 12, the addition of the rainbird water in ASMAT 11 produced a 3.4-dB reduction of the overall level at the array location. A comprehensive discussion of the effectiveness of the water suppression system on the model and the launch tower is expected from the MSFC testing team. Finally, all spectra of Figure 7.4-16 have double or multiple humps that are tell-tale signs of strong reflection from various parts of the test stand. Some of these reflective surfaces, such as the pad and the ground, are

	Document #:	Version:
NASA Engineering and Safety Center Technical Assessment Report	**NESC-RP-09-00597**	**1.0**

Title:	Page #:
Assessment of Microphone Phased Array for Measuring Launch Vehicle Lift-off Acoustics	36 of 47

representative of the launch environment; while the blast curtain is not. It is difficult to separate the impact of these two types of reflections.
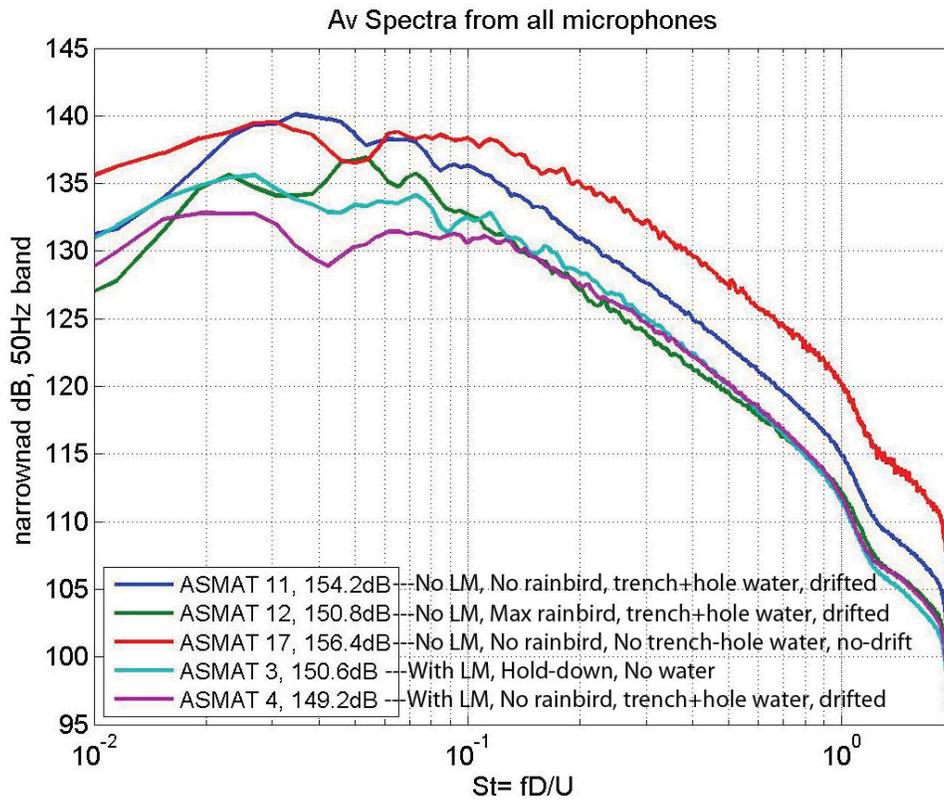
Figure 7.4-16. Comparison of Average Spectra from the Indicated Tests; Average Overall 70 Microphones of the Phased Array

8.0 Findings, Observations, and NESC Recommendation

8.1 Summary and Conclusions

A microphone phased array, comprised of 70-element condenser 0.25-inch-diameter microphones, was successfully used with a minimal loss of sensors in seven ASMAT hotfires. Part of the hardware was custom-built for the test. The processing software was written in the Matlab® platform. The existing array was ruggedized for use in an outdoor rocket test facility. It was built and tested in the ARC acoustics facility, and then shipped to MSFC for rebuilding around test stand TS116. The ASMAT series of static tests used a 5-percent-scaled model of the Ares I vehicle and the launch pad.

8.1.1 Findings

The following significant findings were made:

F-1. The beamformed noise source maps, measured from the horizontal, motor-only test, showed long coherent noise sources modulated by the shock cells that were present in the plume.

F-2. The plume impingement zones were found to be the primary noise-sources in all vertical tests that simulated various altitudes during lift-off.

- As the vehicle was elevated, a part of the plume spilled outside the MLP hole creating an impingement zone.

- Lateral drift of the vehicle further strengthened plume impingement.

F-3. The uncovered part of the trench, the deflector, and the gap around the MLP were major noise sources when no water was used for attenuation.

F-4. The noise sources inside the trench were found to be significantly attenuated via water injection in the MLP hole, on the top of the deflector, and inside the trench.

F-5. Results obtained from one test involving injection of the on-deck water (rainbird) initially showed effectiveness in source mitigation. The motor plume was found to displace water quickly and to reduce the water's effectiveness; albeit the spatial extent of the source was reduced.

F-6. It was found that the current lift-off model (SP8072) fails to account for the impingement noise-sources. There is a need to update this model.

F-7. The phased array (and its sensors), if properly designed and protected, will survive the weather and motor hotfire environments reliably.

F-8. Attempts were made to apply some of the advanced beamforming algorithms to improve the frequency range of the test array. Different sets of difficulties arose for different algorithms when attempts were made to use with the rocket test data. More work is needed to achieve this goal.

8.1.2 Observations

The following observations were identified:

O-1. With the right sets of safeguards, sensitive electronic components of a microphone phased array were found to withstand the harsh environment of an outdoor rocket test facility without any significant problem. In return, the phased array was found to provide previously unavailable insights into the noise sources.

O-2. The 40-inch-diameter array was found to be most effective in resolving noise sources above 2 kHz, which was satisfactory for the present model scale test.

- For application in a full-scale launch where frequencies of interest are below 2 kHz, the array either needs to be placed close to the pad or needs to be larger in size.

8.1.3 NESC Recommendation

The following NESC recommendation was identified and directed towards future use of phased array in lift-off applications:

R-1. For the present test, the array was placed away from the model. Since the noise sources are directional in nature, it is recommended to place the array closer to the model. This will make the noise source maps more relevant for the vehicle development program. *(All Findings)*

9.0 Alternate Viewpoint

There were no alternate viewpoints identified during the course of this assessment by the NESC team or the NRB quorum.

10.0 Other Deliverables

No unique hardware, software, or data packages, outside those contained in this report, were disseminated to other parties outside this assessment.

11.0 Lessons Learned

No applicable lessons learned were identified for entry into the NASA Lessons Learned Information System.

12.0 Definition of Terms

Corrective Actions   Changes to design processes, work instructions, workmanship practices, training, inspections, tests, procedures, specifications, drawings, tools, equipment, facilities, resources, or material that result in preventing, minimizing, or limiting the potential for recurrence of a problem.

Finding

A conclusion based on facts established by the investigating authority.

Lessons Learned

Knowledge or understanding gained by experience. The experience may be positive, as in a successful test or mission, or negative, as in a mishap or failure. A lesson must be significant in that it has real or assumed impact on operations; valid in that it is factually and technically correct; and applicable in that it identifies a specific design, process, or decision that reduces or limits the potential for failures and mishaps, or reinforces a positive result.

Observation

A factor, event, or circumstance identified during the assessment that did not contribute to the problem, but if left uncorrected has the potential to cause a mishap, injury, or increase the severity should a mishap occur. Alternatively, an observation could be a positive acknowledgement of a Center/Program/Project/Organization's operational structure, tools, and/or support provided.

Problem

The subject of the independent technical assessment.

Proximate Cause

The event(s) that occurred, including any condition(s) that existed immediately before the undesired outcome, directly resulted in its occurrence and, if eliminated or modified, would have prevented the undesired outcome.

Recommendation

An action identified by the NESC to correct a root cause or deficiency identified during the investigation. The recommendations may be used by the responsible Center/Program/Project/Organization in the preparation of a corrective action plan.

Root Cause

One of multiple factors (events, conditions, or organizational factors) that contributed to or created the proximate cause and subsequent undesired outcome and, if eliminated or modified, would have prevented the undesired outcome. Typically, multiple root causes contribute to an undesired outcome.

13.0 Acronyms List

ARC   Ames Research Center
ASMAT Ares I Scale Model Acoustics Test
CSM   Cross-Spectral Matrix
DAMAS Deconvolution Approach for the Mapping of Acoustic Sources
dB   Decibel
FY   Fiscal Year
IOP   Ignition Over-Pressure

KSC	Kennedy Space Center
LaRC	Langley Research Center
LM	Launch Mount
MLP	Mobile Launch Platform
MPCV	Multi-Purpose Crew Vehicle
MSFC	Marshall Space Flight Center
MTSO	Management Technical Support Office
NESC	NASA Engineering and Safety Center
NRB	NASA Review Board
PC	Personal Computer
psf	Point-Spread Function
RATO	Rocket-Assist Take Off
SLS	Space Launch System
SRB	Solid Rocket Booster
TDT	Technical Discipline Team

14.0 References

1. Panda, J. and Mosher, R., 2011, "Use of a Microphone Phased Array to Determine Noise Sources in a Rocket Plume," AIAA paper 2011-974, presented at 49th Aerospace Sciences Meeting.

2. Haynes, J., and Kenny, J. R., 2009, "Modifications to the NASA SP-8072 Distributed Source Method II for Ares I Lift-off Environment Predictions," AIAA paper 2009-3160, presented at the 15th AIAA/CEAS Aeroacoustics Conference, Miami, Florida.

3. Plotkin, K. J., Sutherland, L. C., and Vu, B., 2009, "Lift-off Acoustics Predictions for the Ares I Launch Pad," AIAA paper 2009-3163, presented at the 15th AIAA/CEAS Aeroacoustics conference, Miami, Florida.

4. Varnier, J., 2001 "Experimental Study and Simulation of Rocket Engine Free jet Noise," AIAA J. Vol. 39, No. 10, 2001.

5. Eldred, K. M. and Jones, G. W. Jr., 1971 "Acoustic Load Generated by the Propulsion System," NASA SP-8072.

6. Tsutsumi, S., Kato, S., Fukuda, K., Takaki, R., and Ui, K. 2009, "Effect of Deflector Shape on Acoustic Field of Launch Vehicle at Lift-off," AIAA paper 2009-328, presented at the 47th AIAA Aerospace Sciences Meeting, Orlando, Florida.

7. Underbrink, J. R., 2001, "Aeroacoustics Phased Array Testing in Low Speed Wind Tunnels," in *Aeroacoustics Measurements, Springer, Ed. Thomas J. Mueller.*

8. Brooks, T. F. and Humphreys, W. M. Jr., 2006, "A Deconvolution Approach for the Mapping of Acoustic Sources (DAMAS) Determined from Phased Microphone Arrays," *J. Sound & Vib.*, 294, pp. 856-879.

9. Gély, D., Elias, G., Bresson, C., Foulon, H., Radulovic, S, 2000, "Reduction of Supersonic Jet noise. Application to the Ariane 5 Launch Vehicle," AIAA paper 2000-2026, 6th AIAA/CEAS Aeracoustics Conference, Hawaii.

10. Sankaran, S., Ignatius, J. K., Ramkumar, R., Satyanarayana, T. N. V., Chakravarthy, S. R., and Panchapakesan, N.R., 2009, "Suppression of High Mach Number Rocket Jet Noise by Water Injection," J. Spacecraft & Rockets, Vol. 46, No. 6, pp. 1164-1170.

11. Sutherland, L.C., 1993 "Progress and Problems in Rocket Noise Prediction for Ground Facilities," AIAA Paper 93-4383.

12. Dougherty, N. S., Nesman, T. E., Guest, S. H., 1982, "Shuttle SRB Ignition Overpressure: Model Suppression Test Program and Flight Results," presented at the JANNAF 13th Plume Technology Meeting, Houston, Texas, April 27-28, 1982.

13. Dougherty, N. S. and Guest, S. H., 1984, "A Correlation of Scale Model and Flight Aeroacoustic Data for the Space Shuttle Program," AIAA paper 1984-2351, presented at the 9th AIAA Aeroacoustics Conference, Williamsburg, Virginia.

14. Fukuda, K., Tsutsumi, S., Fujii, K., Ui, K., Ishii, T., Oimuna, H., Kazawa, J., Minesugi, K., 2009 "Acoustic Measurement and Prediction of Solid Rockets in Static Firing Tests," AIAA paper 2009-3368.

15. Burnside, N. J., Jaeger, S. M., Reinero, B. R., Horne, W. C., and Soderman, P. T., 2002, "Array Design and Performance for a Large Scale Airframe Noise Study," AIAA paper 2002-2576.

16. Dougherty, R. P., Stoker and R. W., 1998, "Sidelobe Suppression for Phased Array Aeroacoustic Measurements," AIAA-98-2242.

17. Sijtsma, P., "CLEAN-Based on Spatial Source Coherence," 13th AIAA/CEAS Aeroacoustics Conference 28th AIAA Aeroacoustics Conference), AIAA 2007-3436.

18. Dougherty, B., "DAMAS, Eigen values, CLEAN-SC and TIDY," keynote address, AIAA Aeroacoustics Conference, May 2009.

15.0 Appendices

A. Advanced Beamforming Efforts

Appendix A. Advanced Beamforming Efforts

As discussed earlier, the source map obtained via the conventional beamform process has poor resolution at low frequency range, and the presence of many side lobes in the high frequency range, which may appear as pseudo sources. Besides, the uncertainty in the absolute source, amplitude is high in the conventional beamform results. Many of these difficulties are due to the smearing and interference associated with the psf inherent to the array layout. To alleviate such difficulties, in recent times, there have been multiple efforts to deconvolve the psf from the beamformed output. The most straightforward one, DAMAS [ref. 1], involves large matrix manipulation and long computing time. Efforts were made, with limited success, to implement DAMAS. There are multiple other approaches [refs. 8, 16, 17, and 18] with their own shortcomings, such as DAMAS [refs. 2, 16, and 18] and CLEAN-Spatial Correlation (SC) [ref. 17]. Both of these algorithms were attempted during this assessment. In the following mathematical steps, Matlab® implementations and sample results are presented.

A.1 Deconvolution using DAMAS

If there is a noise source at one point in the interrogation grid, the inherent psf of the array spreads its influence to all other grid points. If the distribution of the true source is x_j, $j = 1, 2, \ldots N$, then the conventional beamform level at any grid point j (equation 3) is the following sum:

$$b_j = A_{j1}x_1 + A_{j2}x_2 + \cdots + A_{jj}x_j + \cdots + A_{jN}x_N \qquad (8)$$

Here, A_{j1} is the influence of a source at the grid point 1 to the beamformed map at point j, and similarly for other terms. Every term of the influence matrix $A_{jj'}$ can be calculated based on the original assumption of monopole noise source of unit strength at location j' and the resulting steering vectors:

$$A_{jj'}(f) = \frac{w_j^\dagger W([\ ]_{j'})_{diag=0} W^\dagger w_j}{(\sum W_m)^2 - (\sum W_m)} \qquad (9)$$

The term in parenthesis is the modeled CSM corresponding to a unit monopole source. It can be calculated using steering vectors from the source point j' to every microphone locations $\ell = 1, 2, \ldots M$ as the following:

$$([\ ]_{j'}) = \begin{bmatrix} (w_1^*)w_1 & \cdots & (w_1^*)w_M \\ \vdots & \ddots & \vdots \\ & \cdots & (w_M^*)w_M \end{bmatrix}_{j'} \qquad (10)$$

Succinctly, equation 8 above can be expressed as the following:

$$b_j(f) = \sum_{j'} A_{jj'} x_{j'} \qquad (11)$$

This represents a system of linear equations whose solution should provide amplitude of the true sources x_j. However, the psf varies slowly between grid points, and the rank of the matrix A was found to be significantly low, which indicates that equation 11 can accept many different solutions (uniqueness problem). Brooks and Humphreys [ref. 8] provides an outline of an iterative Gauss-Seidel scheme along with a regularization procedure that was implemented in a Matlab® code. Typical success is shown in Figure A-1. For data collected from anechoic chamber, the scheme was found to converge to desirable solutions, albeit with some effort especially with the multiple speaker data. Finding a converged solution for data taken from the ASMAT stand proved to be far more difficult. To check for the convergence of the solution scheme, the summed-up rms of source fluctuations (x_j) was plotted as a function of the number of iterations. Figure A-1 shows that the deconvolution scheme diverged for the data collected from the horizontal fire test. ASMAT stand created a semi-reverberation environment. Not all reflection sources could be considered into the interrogation region. The monopole assumption of the long coherent noise sources may not be appropriate.
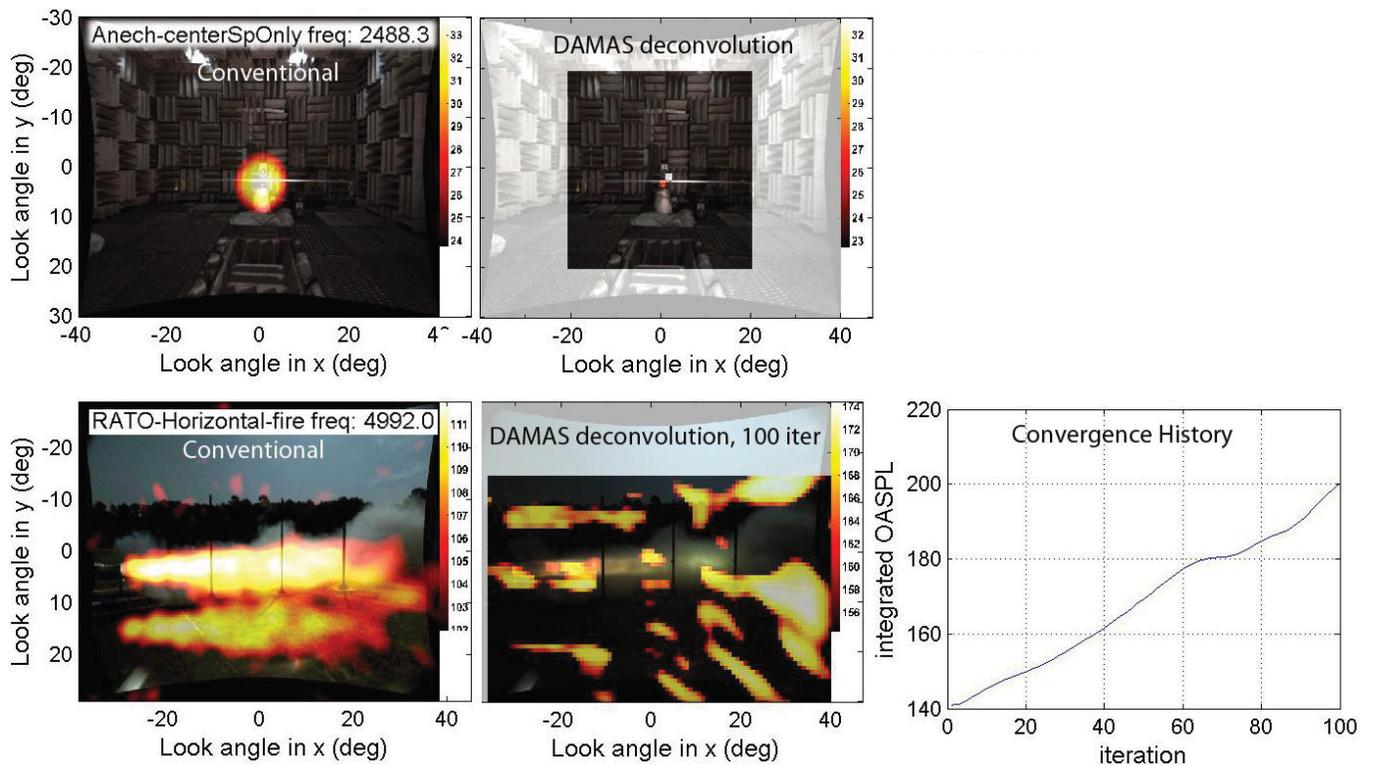
Figure A-1. DAMAS Deconvolution: (top row) a Single Microphone Noise Source in Anechoic Chamber; (bottom row) Plume from Horizontal Motor Fire

A.2 Deconvolution using CLEAN-SC

The CLEAN-SC is a relatively fast and well-understood methodology among many available faster procedures to remove the influence of the psf on the source map. However, one needs to trace the underlying sources in the conventional map before applying CLAEAN-SC. The deconvolution processes work on the conventional map to sharpen the location of the source and to help eliminate the side-lobes.

CLEAN-SC is an improvement over the original CLEAN methodology that is used in radio astronomy. The name CLEAN comes from the progressive buildup of a "clean-map" (C^i) at the expense of a "dirty-map" (D^i). Initially, the dirty-map is the conventional beamform expressed as

$$D^0 = b_j \qquad (12)$$

The process begins with the identification of the location ξ_k and level b_k of the peak noise source in the conventional beamform. The clean-map C^i is started with this location and level

$$C^1 = b_k 10^{-\alpha|\xi_j - \xi_k|^2} \qquad (13)$$

Here α is a smearing factor, without which the sharp peaks may not be detectable in the plots. Next, the expected contribution of an equivalent monopole (of strength b_k located at ξ_k) is subtracted from both the CSM and the dirty-map. The peak locations and levels in this revised dirty-map are transferred to the clean-map. The process is continued until a convergence criterion is met.

Peter Sijtsma's contribution in CLEAN-SC [ref. 17] is an improved procedure to subtract the contribution of the already found source at the peak location. The procedure is based on the coherence values between the peak source b_k at location ξ_k with all other points in the beamformed map. Quintessentially, the psf makes the influence of a point source felt over the entire beamform map. This spread-out part is established via the coherence levels between the source at ξ_k and all other points ξ_j in the map. However, this coherence calculation depends on whether the diagonal terms of the CSM are deleted or not.

When the diagonal elements of the CSM are as measured (not deleted), the coherence is calculated based on the degraded CSM as

$$\Gamma_{jk}^2 = \frac{|b_{jk}|^2}{b_j b_k} \, , \text{ where } b_{jk} = \boldsymbol{w_j}^\dagger \boldsymbol{G}^{(i-1)} \boldsymbol{w_k} \qquad (14)$$

The new degraded dirty-map is calculated by subtracting the coherent part from the earlier version by using

$$D^i = D^{(i-1)}\left(1 - \Gamma_{jk}^2\right) \qquad (15)$$

The degraded CSM is then established by factoring out contribution of an equivalent monopole at ξ_k by using

$$G^i = G^{(i-1)} - b_k\left(w_k\, w_j^\dagger\right) \tag{16}$$

The convergence is achieved when the newly degraded CSM has more energy than the previous iteration. This is given by the expression

$$\left|G^i\right|^2 \geq \left|G^{(i-1)}\right|^2 \tag{17}$$

The final clean-map is simply a sum of peaks found in the earlier iteration plus the final degraded dirty-map, or

$$C^{final} = \sum_i C^i + D^{residual} \tag{18}$$

When the diagonal elements of the CSM are deleted, the coherence value Γ [ref. 2] can become unphysical since the beamform values b_{jj} can even be negative. Equations 14, 15, and 16 can no longer be applied. Instead of directly calculating the coherence (which was ultimately used to establish the degraded CSM, equation 16), Sijtsma specifies an effective steering vector h from the source point ξ_k given by

$$h = \frac{1}{\left(1+w_k^\dagger H\, w_k\right)^{1/2}}\left(\frac{G\, w_k}{b_k} + H\, w_k\right) \tag{19}$$

which is then used to establish the degraded CSM, expressed as

$$G^i = G^{(i-1)} - b_k(h\, h^\dagger - H)$$
$$where\ H = diagonal\ elements\ of\ h\, h^\dagger \tag{20}$$

In the above two equations, h is calculated iteratively starting with an initial value of $h = w_k$. The converged h values are obtained within a few iterations. Unlike the equation 15, the degraded dirty-map is calculated from the degraded CSM as

$$D^i = w_j^\dagger G^i\, w_j \tag{21}$$

which is then used to find out the new peak. The process is continued until the convergence criterion of equation 18 is met. Typically, an acceleration factor (between 0.5 and 0.95) is used to help extract distributed sources with equations 15, 16, and 20.

The above scheme was implemented in Matlab® and at first applied to data from individual speaker sources in the anechoic chamber. Figure A-2 shows a comparison between results from the conventional beamform and CLEAN-SC. The deconvolution procedure significantly localizes the source by removing the influence of the psf. However, neither of them can isolate the three speakers at the lower frequencies, well below the Rayleigh resolution limit. A closer look into the methodologies clarifies this deficiency. The deconvolution procedures start with the peak noise identified in the conventional map (equation 6 above). The location and level of

the peak are due to a sum of effects from all three sources. For frequencies below the Rayleigh resolution, the peak in the conventional beamform does not coincide with a speaker location. This makes the deconvolution procedure start with an incorrect assumption of the peak noise source that ultimately led to incorrect distribution of sources. Fundamentally, for sources spaced closer than the Rayleigh resolution, the summed up field may not have a unique solution for noise sources; that is, multiple combination of locations and amplitudes may provide the same final distribution. Therefore, CLEAN-SC has difficulties overcoming the limitation imposed by the Rayleigh criterion. For frequencies higher than the Rayleigh resolution, Figure A-2 shows that the deconvolution procedures significantly reduce side lobes and dramatically improve beamform results, at least for the point source in an ideal anechoic environment.

The success, however, becomes less expected when applied to the distributed noise source of the horizontal motor test. Figures A-3 and A-4 show comparison between conventional and CLEAN-SC. CLEAN-SC converts the distributed sources into spotty blobs that are unphysical. In addition to removing the side-lobes, which are coherent with the principle noise source, the procedure also takes away the coherent parts of the true sources. No attempts were made to apply CLEAN-SC to the rest of the ASMAT data.
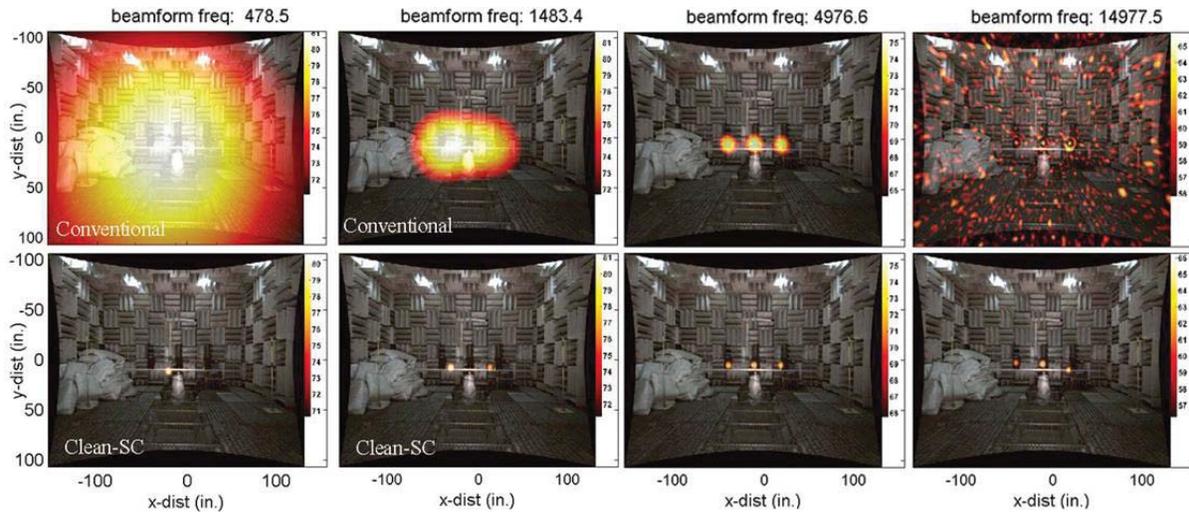

Figure A-2. Comparative Study of Beamforming at the Indicated Frequencies via the Two Indicated Methodologies

		Document #:	Version:
![NASA logo]	**NASA Engineering and Safety Center Technical Assessment Report**	**NESC-RP-09-00597**	**1.0**
Title:			Page #:
	Assessment of Microphone Phased Array for Measuring Launch Vehicle Lift-off Acoustics		47 of 47
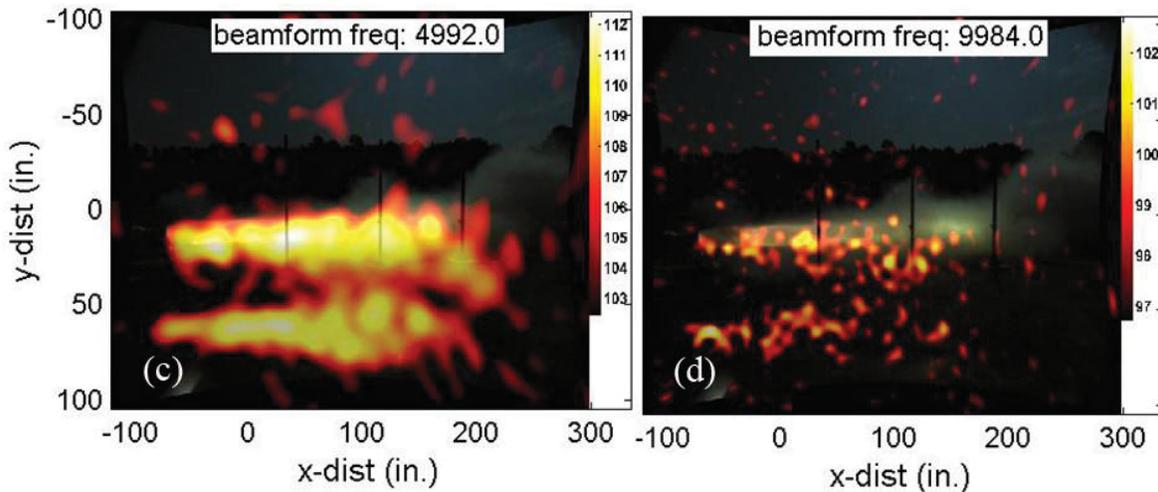
Figure A-3. Conventional Beamform Image of the Noise Source Distribution on the Rocket Plume at the Indicated Frequencies
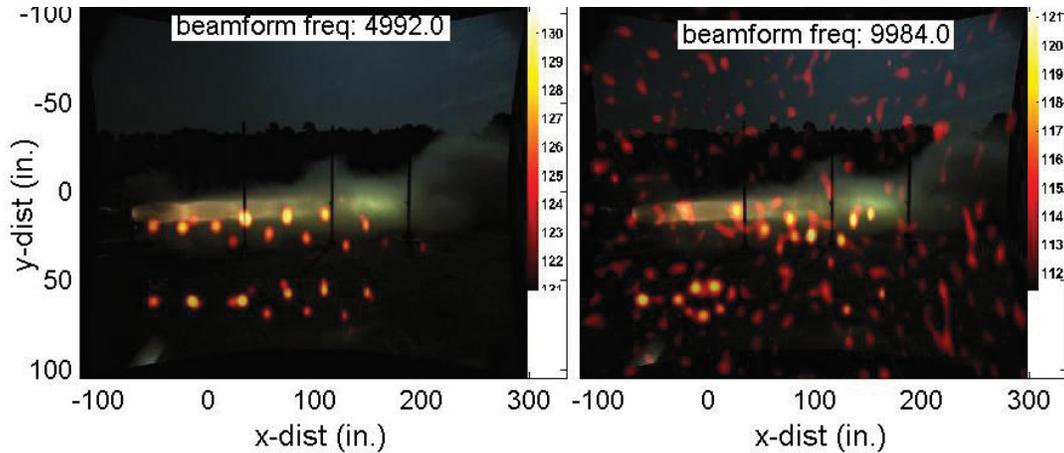
Figure A-4. CLEAN-SC Beamform Images at the Indicated Frequencies

REPORT DOCUMENTATION PAGE					*Form Approved* *OMB No. 0704-0188*

1. REPORT DATE *(DD-MM-YYYY)*	2. REPORT TYPE	3. DATES COVERED *(From - To)*
01-04-2012	Technical Memorandum	December 2009 - March 2012

4. TITLE AND SUBTITLE

Assessment of Microphone Phased Array for Measuring Launch Vehicle Lift-off Acoustics

5a. CONTRACT NUMBER

5b. GRANT NUMBER

5c. PROGRAM ELEMENT NUMBER

6. AUTHOR(S)

Garcia, Roberto

5d. PROJECT NUMBER

5e. TASK NUMBER

5f. WORK UNIT NUMBER

869021.05.07.01.11

7. PERFORMING ORGANIZATION NAME(S) AND ADDRESS(ES)

NASA Langley Research Center
Hampton, VA 23681-2199

8. PERFORMING ORGANIZATION REPORT NUMBER

L-20138 NESC-RP-09-00597

9. SPONSORING/MONITORING AGENCY NAME(S) AND ADDRESS(ES)

National Aeronautics and Space Administration
Washington, DC 20546-0001

10. SPONSOR/MONITOR'S ACRONYM(S)

NASA

11. SPONSOR/MONITOR'S REPORT NUMBER(S)

NASA/TM-2012-217563

12. DISTRIBUTION/AVAILABILITY STATEMENT

Unclassified - Unlimited
Subject Category 71 - Acoustics
Availability: NASA CASI (443) 757-5802

13. SUPPLEMENTARY NOTES

14. ABSTRACT

The specific purpose of the present work was to demonstrate the suitability of a microphone phased array for launch acoustics applications via participation in selected firings of the Ares I Scale Model Acoustics Test. The Ares I Scale Model Acoustics Test is a part of the discontinued Constellation Program Ares I Project, but the basic understanding gained from this test is expected to help development of the Space Launch System vehicles. Correct identification of sources not only improves the predictive ability, but provides guidance for a quieter design of the launch pad and optimization of the water suppression system. This document contains the results of the NASA Engineering and Safety Center assessment.

15. SUBJECT TERMS

Ares I Scale Model Acoustics Test; microphone phased array; vibro-acoustics; NASA Engineering and Safety Center

16. SECURITY CLASSIFICATION OF:			17. LIMITATION OF ABSTRACT	18. NUMBER OF PAGES	19a. NAME OF RESPONSIBLE PERSON
a. REPORT	b. ABSTRACT	c. THIS PAGE			STI Help Desk (email: help@sti.nasa.gov)
U	U	U	UU	52	19b. TELEPHONE NUMBER *(Include area code)* (443) 757-5802

Standard Form 298 (Rev. 8-98)
Prescribed by ANSI Std. Z39.18